Remote Sensing of Environment 166 (2015) 8–21

Contents lists available at ScienceDirect

Remote Sensing of Environment

journal homepage: www.elsevier.com/locate/rse

Global sensitivity analysis of the SCOPE model: What drives simulated canopy-leaving sun-induced fluorescence?

Jochem Verrelst [a,*], Juan Pablo Rivera [a], Christiaan van der Tol [b], Federico Magnani [c], Gina Mohammed [d], Jose Moreno [a]

[a] Image Processing Laboratory, Department of Earth Physics and Thermodynamics, University of Valencia, C/Catedrático José Beltrán 2, E-46980 Paterna, Valencia, Spain
[b] Department of Water Resources, Faculty ITC, University of Twente, P.O. Box 217, 7500 AE Enschede, The Netherlands
[c] Department of Agricultural Sciences, University of Bologna, Bologna, Italy
[d] P&M Technologies, 66 Millwood Street, Sault Ste. Marie, Ontario, Canada

ARTICLE INFO

Article history:
Received 23 December 2014
Received in revised form 25 May 2015
Accepted 1 June 2015
Available online 11 June 2015

Keywords:
Sun-induced fluorescence
Global sensitivity analysis
SCOPE
Light transfer
Scattering
Photosynthesis
FLEX

ABSTRACT

This study provides insight into the key variables that drive sun-induced chlorophyll fluorescence (SIF) emanating from vegetation canopies, based on a global sensitivity analysis (GSA) of the Soil-Canopy Observation of Photosynthesis and Energy (SCOPE) balance model. An updated version of the SCOPE model was used here (v1.53) which contains novel leaf physiological modules for determination of the steady state fluorescence yield: a photosynthesis model coupled with (a) submodels having empirically derived relationships, identified as TB12 for unstressed and TB12-D for drought conditions and (b) a mechanistic (MD12) submodel based on theoretical relationships. By inspecting Sobol's total order (main effect and all the interactions) sensitivity index (S_{Ti}) rankings, the influential and non-influential variables were determined. Two experiments were conducted for the different leaf physiology modules in SCOPE considering (1) only vegetation variables, and (2) all SCOPE variables, i.e., including micrometeorological, aerodynamic and geometry variables.

Considering TB12-D S_{Ti} results using only vegetation input variables, the canopy-leaving broadband (641–800 nm) SIF variability was determined mainly by leaf optical properties and canopy structural variables. The most important variables were (with decreasing importance) leaf chlorophyll content (Cab), leaf inclination (LIDFa) and leaf area index (LAI). These three variables alone determined 77.9% of the SIF variability. V_{cmo}, the variable related to photosynthetic capacity, determined 11.4% of overall SIF variability, and its importance declined considerably when moving from the first emission peak (SIF_{red}; with maximal relevance of 17.9% at 676 nm) to the second emission peak (SIF_{NIR}; e.g., 9.6% at 740 nm). Stronger relationships with V_{cmo} were obtained when retrieving the full broadband SIF flux and calculating total fluorescence yield (F_{yield}, determined as the integral of the hemispherical broadband SIF flux divided by the total absorbed PAR), of which 35% of the variability was influenced by V_{cmo}. Using the TB12 submodel, the major drivers of SIF flux were similar to TB12-D except that V_{cmo} accounted for very little (<2%) variability. The MD12 submodel identified the components of long-term PSII photoprotection and photodamage as the dominant factors for SIF variability: these two variables alone accounted for 51.4% of the variability of SIF flux and 61% of F_{yield}, whereas V_{cmo} explained only 9.7% and 10.9% of variability in SIF flux and F_{yield}, respectively.

Analysis of the relative importance of all SCOPE variables revealed that in addition to the key vegetation variables, micrometeorological variables were important in driving SIF variability, especially incoming shortwave radiation (Rin) and to a lesser extent air temperature (Ta), atmospheric vapor pressure (ea) and atmospheric CO_2 concentration (Ca). Their impact further reduced the relative importance of V_{cmo}.

The GSA experiments led to the following conclusions: (1) explicit knowledge of key variables driving the SIF flux is essential in order to achieve unbiased SIF interpretation related to photosynthetic activity at local and global scales; (2) information related to photosynthetic activity is found more in the first emission peak (SIF_{red}) than in the second peak (SIF_{NIR}), and more in the full broadband SIF emission, which allows calculation of F_{yield}, than in individual wavebands.

* Corresponding author at: Laboratory of Earth Observation (LEO), Image Processing Laboratory (IPL), Science Park, BOX 22085, University of Valencia, 46071 Paterna, Valencia Spain.
E-mail address: jochem.verrelst@uv.es (J. Verrelst).

http://dx.doi.org/10.1016/j.rse.2015.06.002
0034-4257/

1. Introduction

Sun-induced fluorescence (SIF) emitted by photosystems I and II is one of the three de-excitation mechanisms of energy captured by light harvesting pigments in plants. It competes with photochemical processes and thermal decay (Krause & Weis, 1991). Although the direct link with photosynthesis is not trivial (Meroni et al., 2009) due to the variability of thermal decay, SIF emitted by vegetation is seen as a meaningful indicator of instantaneous plant photosynthetic activity (e.g., carbon fixation), and possibly gross primary productivity (GPP) at the ecosystem scale (Porcar-Castell et al., 2014). A major advantage of the SIF signal is that it is a more physiologically related signal than reflectance, and moreover it originates uniquely from vegetation. While much of the broadband reflectance signal reveals rather slow-changing structural aspects of leaf composition, leaf area and vegetation canopy cover fraction (Rautiainen et al., 2010; Verrelst et al., 2012), SIF represents a more finely-tuned physiological signal with a diurnal dynamic (Amoros-Lopez et al., 2008; Flexas et al., 2002; Zarco-Tejada, Morales, Testi, & Villalobos, 2013). Another dynamic metric is the well-known Photochemical Reflectance Index (or Physiological Reflectance Index, PRI) (Gamon, Penuelas, and Field, 1992) which is correlated with the carotenoid xanthophyll cycle.

Although the emitted canopy-leaving SIF flux is relatively small compared to reflected sunlight (about 1–5% in the near infrared, NIR), it is a broadband spectrum within the 650–800 nm spectral window with two emission maxima: in the red around 685 nm and in the NIR around 740 nm (Baker, 2008; Papageorgiou & Govindjee, 2004). With the development of hyperspectral sensors, the retrieval of SIF has become a novel area of research (Alonso et al., 2007; Guanter et al., 2010; Meroni et al., 2009, 2010) aimed primarily at mapping SIF from site-specific (Damm et al., 2014; Daumard et al., 2012; Moya, Daumard, Moise, Ounis, & Goulas, 2006; Perez-Priego, Zarco-Tejada, Miller, Sepulcre-Canto, & Fereres, 2005; Zarco-Tejada, Gonzalez-Dugo, & Berni, 2012; Zarco-Tejada, Morales, et al., 2013) to the global scale (Frankenberg et al., 2011; Guanter et al., 2012; Joiner et al., 2011). Regardless of the applied scales, current retrieval approaches exploit only one band, which is mostly found in the second fluorescence emission peak, in the 730–770 nm window.

Using retrievals of NIR fluorescence (SIF_{NIR}), a top–down approach has been followed by the global SIF mapping community, whereby meaningful interpretations of SIF_{NIR} retrievals have been sought, typically to link SIF_{NIR} with GPP through empirical relationships (Frankenberg et al., 2011; Guanter et al., 2012, 2014). It is known that SIF is affected by various factors including chlorophyll content, photochemistry, non-photochemical quenching, and leaf and canopy optical characteristics which, in turn, are influenced by diverse biological, environmental, and atmospheric factors (Lichtenthaler & Rinderle, 1988; Malenovský, Mishra, Zemek, Rascher, & Nedbal, 2009; Porcar-Castell et al., 2014; Rascher et al., 2009). For example, the broadband SIF flux propagated through foliage is also subjected to internal absorption and scattering effects. From a bottom–up perspective, scattering and re-absorption effects continue through the canopy, potentially exerting significant effects on vegetation SIF measured remotely. Such drivers of within-leaf and canopy radiative transfer (RT) fluxes have been largely unstudied under natural sunlight conditions. Furthermore, the interplay of these phenomena with meteorological variables such as solar irradiance, air temperature, and air humidity or the factors defining the illumination and observation geometry, are known to affect the radiative transfer of the SIF flux at larger scales (Drusch & FLEX-Team, 2008; Guanter et al., 2010). These effects are qualitatively known, but their relative importance, taking all variables and their interactions into account, remains obscure.

The empirical approaches for SIF_{NIR}–GPP relations that have hitherto been used have demonstrated the potential of the SIF_{NIR} signal. The need for disentangling the complex interplay between changing surface properties and meteorological effects from meaningful information related to photosynthesis nevertheless remains (Damm et al., 2014). The presently available satellite fluorescence products are limited in spatial resolution, and therefore not sufficient for this task.

With the purpose of deriving a deeper understanding of SIF and its relationship to photosynthetic activity at the global scale, the European Space Agency (ESA) is currently conducting Phase A/B1 evaluations of a candidate Earth Explorer mission dedicated to measurement of SIF in terrestrial vegetation. The Fluorescence Explorer (FLEX) satellite, equipped with a Fluorescence Imaging Spectrometer (FLORIS) onboard, is proposed to operate in a tandem mission with ESA's Sentinel-3 satellite, the latter to provide atmospheric and land surface data needed for atmospheric corrections and accurate SIF characterizations. Several scientific and industrial studies have been completed by ESA to establish scientific benchmarks for the FLEX mission. One such project was the FLEX/Sentinel-3 Tandem Mission Photosynthesis Study (Mohammed et al., 2014), which investigated the potential of SIF for quantifying photosynthesis, vegetation health, and stress status. As part of that study, the SCOPE (Soil-Canopy Observation, Photosynthesis and Energy Balance) model (Van der Tol, Verhoef, Timmermans, Verhoef, & Su, 2009) has been extended with new leaf fluorescence modules (resulting in Version 1.53). SCOPE combines the functionality of a Soil–Vegetation–Atmosphere (SVAT) model with radiative transfer of reflected and emitted (thermal and fluorescent) radiation, and enables to facilitate the interpretation of SIF retrievals from space towards estimation of photosynthetic properties, e.g., through inversion of FLEX SIF data (Mohammed et al., 2014).

A major benefit of coupling leaf physiological models with leaf and canopy RT models is that it enables identification and quantification (ranking) of influential and less influential variables governing the fluorescence signal emitted by the canopy, through a sensitivity analysis. Elucidating the main drivers of SIF variability can lead to an improved understanding of the canopy SIF and photosynthesis dynamics, both in time at a single site and globally. By identifying variables of lesser influence, models can be greatly simplified, which facilitates inversion applications. A global sensitivity analysis (GSA) is an excellent method to quantify the relative importance of each input variable to model outputs (e.g., SIF), and it can help set safe default values for less influential variables (Saltelli, Tarantola, & Chan, 1999). In the present analysis, the driving input variables shaping the SIF emission are identified for the SCOPE model, not only for a single wavelength but for the complete broadband spectral emission region.

The main objectives here were twofold: first, to summarize the latest configuration of the SCOPE model (version 1.53); and second, to present a variance-based GSA quantifying the relative importance of input variables to SIF outputs from the SCOPE model. The GSA analysis has been separated into two parts. First, a dedicated GSA indicative of a single scene acquisition is conducted. In this case, only variation of vegetation variables were considered (whereas meteorological data were kept constant, representing spatial variability in a small area), thus providing an improved understanding of SIF propagation through the canopy. Second, to bridge the present gap between small scale field studies and global observations, a more general GSA was conducted that considered all SCOPE variables. These include micrometeorological and geometry variables, and taking into account their full range of occurrence globally. This second analysis contributes to an improved understanding of spatial variability in global SIF maps and of the challenges and needs for photosynthetic activity monitoring.

2. SCOPE and A-SCOPE models

As summarized by Zarco-Tejada, Catalina, González, and Martín (2013), early modeling work of SIF was carried out within an ESA study by Miller et al. (2003), in which the vegetation fluorescence canopy model FluorMOD was developed (Miller et al., 2005), consisting of the leaf model FluorMODleaf (Pedrós, Goulas, Jacquemoud, Louis, & Moya, 2010; Pedrós, Jacquemoud, Goulas, Louis, & Moya, 2004;

Pedrós, Moya, Goulas, & Jacquemoud, 2008) and the canopy model FluorSAIL (Verhoef, 2004). FluorMOD was useful for evaluating whether the fluorescence signal superimposed onto leaf and canopy reflectance spectra could be discriminated. Subsequent efforts investigated SIF retrieval accuracy in response to relevant sensor properties – namely spectral sampling interval, spectral resolution, signal to noise and spectral shift – and various fluorescence retrieval methods (Damm et al., 2011). These experimental and modeling advances were foundational to the development of SCOPE (Van der Tol, Verhoef, & Rosema, 2009; Van der Tol, Verhoef, Timmermans, et al., 2009), an integrated leaf–canopy fluorescence–temperature–photosynthesis model.

Within the framework of the Photosynthesis Study (Mohammed et al., 2014), SCOPE was updated as described below. In addition, a graphical user interface called Automated-SCOPE (or A-SCOPE) was built for the updated SCOPE model. This GUI streamlines inputs and outputs of the simulations, thereby expediting the generation of large look-up tables (LUT). The A-SCOPE software package is integrated into an in-house developed ARTMO (Automated Radiative Transfer Models Operator) platform (Verrelst, Alonso, Rivera Caicedo, Moreno, & Camps-Valls, 2013) which enables operation of a multitude of leaf and canopy radiative transfer models.

2.1. SCOPE

SCOPE is a vertical (1-D) integrated radiative transfer and energy balance model (Van der Tol, Verhoef, Timmermans, et al., 2009). It calculates radiation transfer in a multilayer canopy, in order to obtain reflectance and fluorescence in the observation direction as a function of the solar zenith angle and leaf inclination distribution.

The fate of irradiance and the distribution of absorbed radiation within the canopy is calculated with the Scattering of Arbitrarily Inclined Leaves' (SAIL) model (Verhoef, 1984). The distribution of absorbed radiation is further used in a micrometeorological representation of the canopy for the calculation of photosynthesis, fluorescence, latent and sensible heat. The fluorescence and thermal radiation emitted by individual leaves is finally propagated through the canopy, again with the SAIL modeling concept (Van der Tol, Verhoef, Timmermans, et al., 2009).

Apart from the canopy radiative transfer modules, the following leaf-level modules are relevant:

1. A leaf radiative transfer module that calculates absorbed photosynthetically active radiation (APAR), reflectance and fluorescence spectra as a function of the irradiance spectrum and the leaf composition. The module calculates excitation–emission probability matrices for both sides of the leaf.
2. A biochemical module that calculates the photosynthesis rate and the fraction of absorbed light returning as fluorescence, as a function of APAR, temperature, relative humidity, the concentrations of CO_2 and O_2.

The separation of the two modules has the advantage that the effects of scattering and re-absorption due to leaf structure (module 1) can be calculated in advance. This calculation does not need to be repeated when weather conditions change, leading to greater computational efficiency. The relative fluorescence is coupled with the radiative transfer module in the following way:

$$F = \varepsilon F_{0(PSII)} + F_{0(PSI)} \quad (1)$$

where F_0 is the fluorescence spectrum ($W\,m^{-2}\,\mu m^{-1}\,sr^{-1}$) as calculated with the leaf radiative transfer module for the dark adapted, low light condition, and ε is a fluorescence amplification factor, calculated with the biochemical routine as the ratio of the steady state (Ft) to the dark adapted fluorescence (Fo). It links the biochemical routine (which calculates relative fluorescence changes due to weather, but not the absolute fluorescence in energy units), and the Fluspect model (which calculates the absolute fluorescence as affected by leaf structure, but not the weather induced fluorescence variations). The factor ε thus accounts for the rapid physiological regulation of fluorescence, whereas F_0 accounts for leaf structure and chemical composition. Note that the adjustment by means of ε is only carried out for the fluorescence contribution of PSII, while the fluorescence of PSI is considered unaffected by biochemistry. The spectral shapes of F_0 have been obtained from Franck, Juneau, and Popovic (2002), who originally normalized the spectra by the integral over the fluorescence spectrum. In SCOPE they are rescaled such that the spectrally integrated emission of PSII is 5× that of PSI (when $\varepsilon = 1$). As we show later, the assumption of a constant PSI causes the sensitivity to ε (and thus to biochemical factors) to decline with increasing fluorescence wavelength, since the contribution of PSI grows with wavelength (Franck et al., 2002).

In the Photosynthesis Study (Mohammed et al., 2014), the following updates were made to SCOPE:

- In the original version of SCOPE, the leaf radiative transfer model PROSPECT (Jacquemoud & Baret, 1990) was used for fluorescence, whereas the fluorescence radiative transfer within the leaf had to be calculated outside the model, and provided separately as input. In SCOPE 1.53, the Fluspect model, which is an extension of the PROSPECT model, was implemented for the calculation of leaf reflectance and fluorescence spectra.
- One mechanistic and two empirical modules for ε were implemented (see Section 2.1.2).
- Two fluorescence contributions have been distinguished: that from photosystem I (PSI), and that from photosystem II (PSII). The contribution of PSII responds readily to physiological regulation (i.e., has a variable ε), whereas the contribution of PSI is proportional to the APAR spectrum and independent of stress factors (i.e., $\varepsilon = 1$) insofar as it is not affected by rapid adjustments in photochemical and non-photochemical quenching (Porcar-Castell et al., 2014).

This updated SCOPE model has recently been used to retrieve a photosynthetic property, the carboxylation capacity (V_{cmo}), from satellite estimates of SIF (Zhang, Liang, Zhou, Wu, & Zhao, 2014; Zhang et al., 2014).

2.1.1. Inclusion of Fluspect

The Fluspect model calculates fluorescence spectra for the illuminated ('backward fluorescence') and the shaded side ('forward fluorescence') of the leaf, from PROSPECT outputs of leaf reflectance and fluorescence based on the Kubelka–Munk equation. The model calculates fluorescence excitation–emission matrices, which express the fraction of incident light of wavelength i (400–750 nm with 1 nm resolution) resulting in fluorescence of wavelength j (640–850 nm with 1 nm resolution). Hence, the emitted fluorescence for the top and bottom side of the leaf depends on the irradiance of a leaf (which in turn depends on its position and orientation in the canopy) and the composition of the leaf as described with the PROSPECT parameters:

$$F_0 = \mathbf{M}I \quad (2)$$

where $\mathbf{M}$ is the fluorescence matrix, and I the irradiance vector. Fluspect produces a separate $\mathbf{M}$ for forward and backward fluorescence. Furthermore, in the implementation of Fluspect in SCOPE, separate matrices for PSI and PSII are calculated. This enables the calculation of fluorescence in upward and downward direction in the canopy from upward and a downward irradiance fluxes.

2.1.2. Update of leaf physiological modules

Several new leaf physiological routines have been introduced for two purposes: (1) to improve the description of fluorescence quenching mechanisms and (2) to improve the comparability with existing global

land surface models. The stomatal model of Cowan and Farquhar (1977) has been replaced by the more widely used model of Ball, Woodrow, and Berry (1991). Two alternative representations of photosynthesis can be selected, based either on the models of Farquhar, von Caemmerer, and Berry (1980) (for C3 species) and Von Caemmerer (2013) (for C4 species), or on the model by Collatz, Ball, Grivet, and Berry (1991), Collatz, Ribas-Carbo, and Berry (1992) that is also used in land surface models such as the Community Land Model, CLM (Bonan, 1996) and the Simple Biosphere 2 model, SiB2 (Sellers et al., 1996). A relevant feature, the carboxylation capacity at optimum temperature, V_{cmo}, has been allowed to vary with depth in the canopy following Sellers, Berry, Collatz, Field, and Hall (1992); potential electron transport rate (Jmo) has been assumed to be proportional to V_{cmo} (Leuning, 1997), and both are scaled in response to leaf temperature.

For fluorescence yield (F_{yield}), alternative descriptions have been formulated. Two of these (Van der Tol, Berry, Campbell, & Rascher, 2014), referred hereon as TB12 and TB12-D, are expressions for the F_{yield} calibrated to a number of datasets collected in field and laboratory experiments. These modules describe the relationship between photochemical yield and fluorescence yield empirically for nonstressed, ideal conditions under variable light and CO_2 concentrations (TB12), and for variable drought levels under high light conditions (TB12-D). The third MD12 module (Dayyoub, 2011; Magnani et al., 2009) has a more explicit parameterization of fluorescence quenching mechanisms. In its most recent development (Mohammed et al., 2014), the module also incorporates the effects on photosynthesis and fluorescence of seasonal changes in PSII photoinhibition and sustained, dark-adapted NPQ (Porcar-Castell, 2011). The MD12 module is not limited to the empirical calibration of the TB12 models, and is therefore able to reproduce intermediate conditions using (compared to the TB12 models) two additional variables, those being rate constant of sustained thermal dissipation (kNPQs) and the fraction of functional reaction centers (qLs) (Porcar-Castell, 2011).

2.1.3. Model outputs at leaf and canopy level

The coupled Fluspect and leaf physiological module provides leaf reflectance and SIF spectra at two sides of the leaf of PSI and PSII (Fig. 1). With varying input, the magnitude of the leaf SIF changes (Fig. 2). Chlorophyll content (Cab) has a profound effect on the shape of the spectra, whereas other factors, such as irradiance and photosynthetic capacity, affect the overall level, and have an additional small effect on the spectral shape due to the variable PSII yield (variable ε). The canopy radiative transfer module further calculates the top-of-canopy (TOC) SIF radiance in the observation direction. A new feature in version 1.53 (compared to the original version) is that the hemispherically integrated SIF flux is calculated as well, in analogy to thermal radiation.

3. Global sensitivity analysis

Sensitivity analysis (SA) evaluates the relative importance of each input variable in a model and can be used to identify the most influential variables affecting model outputs (Saltelli et al., 1999; Wainwright, Finsterle, Jung, Zhou, & Birkholzer, 2014). SA can be applied with radiative transfer (RT) models to identify the key determinants of outputs such as fluorescence, reflectance, etc. Less influential variables can also be identified and be safely set to default values under relatively wide ranges of conditions (Cariboni, Gatelli, Liska, & Saltelli, 2007). In general, SA methods may be categorized as either local or global. Local SA methods often are referred to as "one-factor-at-a-time" (OAT), because they involve changing one input variable at a time while holding all others at their central values, then measuring variation in the outputs. A drawback of OAT methods is that they are informative only at the central point where the calculation is executed and do not encompass the entire input variable space. Thus, local SA methods are inadequate for analyzing complex models having many variables, and they may be highly dimensional and/or non-linear (Nossent, Elsen, & Bauwens, 2011; Saltelli & Annoni, 2010; Yang, 2011). The SVAT model SCOPE would be a typical example of a complex RT model necessitating use of a global SA approach.

Unlike local SA, global SA explores the full input variable space. The contribution of each input variable to the variation in outputs is averaged over the variation of all input variables, i.e., all input variables are changed together (Saltelli et al., 1999). The most popular variance-based methods include the Fourier Amplitude Sensitivity Test (FAST) (Cukier, Fortuin, Shuler, Petschek, & Schaibly, 1973; Xu & Gertner, 2007), the Sobol' method (Sobol', 1990), and a modified version of the Sobol' method proposed by Saltelli et al. (2010). Global SA studies have been applied to several different RT models to disentangle input–output relationships. One of the first global SA studies was applied to the PROSAIL (PROSPECT & SAIL) model using an extended version of FAST (Bowyer & Danson, 2004). Similarly, the sensitivity of the 11 variables of a PROSPECT-based Dorsiventral Leaf Model (DLM) was assessed based on Sobol's method (Stuckens, Verstraeten, Delalieux, Swennen, & Coppin, 2009). Recently, Mousivand, Menenti, Gorte, and Verhoef (2014) used Saltelli's method to analyze the sensitivities of a full SVAT model based on the coupling of SLC (Soil–Leaf–Canopy) with the atmospheric model MODTRAN. Altogether, all these studies analyzed variability in leaf or canopy reflectance outputs (or propagated to top-of-atmosphere (TOA) radiance in the case of Mousivand et al. (2014)). In this paper we applied a variance-based global SA to SCOPE reflectance and, for the first time, to SIF outputs. Saltelli's method (Saltelli et al., 2010) was used, which has been demonstrated to be effective in identifying both the main sensitivity effects (first-order effects) (the contribution to the variance of the model output by each input variable) and total sensitivity effects (the first-order effect plus interactions with other input variables) of input variables (Song, Bryan, Paul, & Zhao, 2012). A GUI toolbox with the equations of Saltelli has been created within the ARTMO framework (http://ipl.uv.es/artmo/). The so-called 'GSA toolbox' is freely available and enables the user to autonomously apply GSA exercises to available RTMs.

3.1. Variance-based global sensitivity analysis

In general, variance-based SA methods aim to quantify the amount of variance that each input variable contributes to the unconditional variance of the model output. In the Sobol' technique, these amounts, caused either by a single variable or by the interaction of two or more variables, are expressed as Sobol' sensitivity indices (Nossent et al., 2011). A description according to Song et al. (2012) follows. Formally, given a model $Y = f(X)$, where Y is the model output, $X = (X_1, X_2,\ldots,X_k)$ is the input parameter vector. A variance decomposition of f suggested by Sobol' (1990) is:

$$V(Y) = \sum_{i=1}^{k} V_i + \sum_{i=1}^{k}\sum_{J=i+1}^{k} V_{ij}\ldots + V_{1,\ldots,k} \quad (3)$$

where X is rescaled to a k-dimensional unit hypercube Ω^k, $\Omega^k = |X|0 \le X_i \le 1, \quad i = 1,\ldots,k\}$; $V(Y)$ is the total unconditional variance; V_i is the partial variance or 'main effect' of X_i on Y and given by $V_i = V[E(Y|X_i)]$; and V_{ij} is the joint impact of X_i and X_j on the total variance minus their first-order effects.

Here, the first-order sensitivity index S_i and total effect sensitivity index S_{Ti} are given as (Saltelli et al., 2008):

$$S_i = \frac{V_i}{V(Y)} = \frac{V[E(Y|X_i)]}{V(Y)} \quad (4)$$

and

$$S_{Ti} = S_i + \sum_{J\neq i} S_{ij} + \cdots = \frac{E[V(Y|X_{\sim i})]}{V(Y)} \quad (5)$$

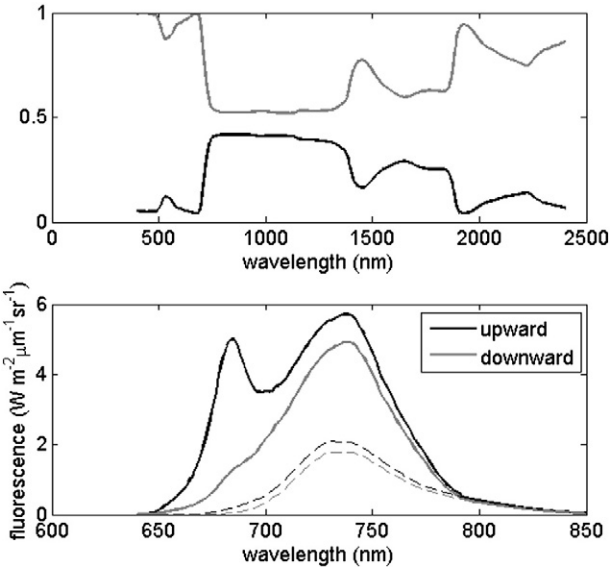

Fig. 1. Top: Simulated leaf transmittance (gray) and reflectance (black) spectra. Bottom: simulated leaf SIF spectra for typical midday conditions. Dashed lines indicate the PSI contribution, whereas solid lines indicate total SIF (PSI + PSII contributions).

where $X_{\sim i}$ denotes variation in all input parameters and X_i, S_{ij} is the contribution to the total variance by the interactions between parameters.

Following Saltelli et al. (2010) to compute S_i and S_{Ti}, two independent input parameter sampling matrices P and Q with dimension (N, k) were created, where N is the sample size and k is the number of input parameters. Each row in matrix P and Q represents a possible value of X. The variable ranges in the matrices are scaled between 0 and 1. The Monte Carlo approximations for V(Y), S_i and S_{Ti} are defined as follows (Jansen, 1999; Nossent et al., 2011; Saltelli et al., 2010):

$$\hat{f}_0 = \frac{1}{N}\sum_{j=1}^{N} f(P)_j \tag{6}$$

$$\hat{V}(Y) = \frac{1}{N}\sum_{J=1}^{N}\left(f(P)_j\right)^2 - \hat{f}_0^2 \tag{7}$$

$$\hat{S}_i = \frac{1}{N}\sum_{j=1}^{N}\frac{f(Q)_j\left(f\left(P_Q^{(i)}\right)_j - f(P)_j\right)}{\hat{V}(Y)} \tag{8}$$

and

$$\widehat{S_{Ti}} = \frac{1}{2N}\sum_{J=1}^{N}\frac{\left(f(p)_j - f\left(P_Q^{(i)}\right)_j\right)^2}{\hat{V}(Y)} \tag{9}$$

where $\hat{\cdot}$ is the estimate; $\hat{f}_0$ is the estimated value of the model output; $P_Q^{(i)}$ represents all columns from P except the i-th column which is from Q, using a radial sampling scheme (Campolongo, Saltelli, & Cariboni, 2011; Saltelli & Annoni, 2010). To compute S_i and S_{Ti} simultaneously, a scheme suggested by Saltelli (2002) was used which reduced the model runs to $N(k + 2)$.

To sample the P and Q matrices the Sobol' quasi-random sampling technique (Sobol', 1967) was used. This sequence helps to distribute the sampling points as uniformly as possible in the variable space to avoid clustering, and increases the convergence rate (Saltelli et al., 2008). Therefore, the use of these sequences enhances the convergence of the Monte Carlo integrals. Whereas the Monte Carlo integration, and thus the Sobol' SA, normally converges at a rate of $1/\sqrt{n}$, the Sobol' quasi-random sampling enhances this to almost $1/n$ (Kucherenko, Rodriguez-Fernandez, Pantelides, & Shah, 2009; Nossent et al., 2011).

4. Experimental setup

Because SCOPE v1.53 is equipped with over 30 input variables (Table 1) and offers a wide range of output products (organized according to fluxes, radiation, reflectance, spectrum, surface temperature, SIF, vertical profiles), all types of input–output sensitivity studies can be conducted. Here, the focus was only on SIF output, i.e., the SIF broadband signal from 641 to 800 nm and the derived product F_{yield}. F_{yield} was calculated as the integral of the hemispherical SIF broadband signal divided by the total absorbed PAR by the plants (APAR). F_{yield} serves to normalize SIF radiance, which is known to be strongly associated with incoming and absorbed irradiance (e.g., Meroni et al., 2011; Srivastava, Greppin, & Strasser, 1995). This makes it possible to relate fluorescence to photochemical yields in order to ascertain photosynthetic efficiency (Louis et al., 2005).

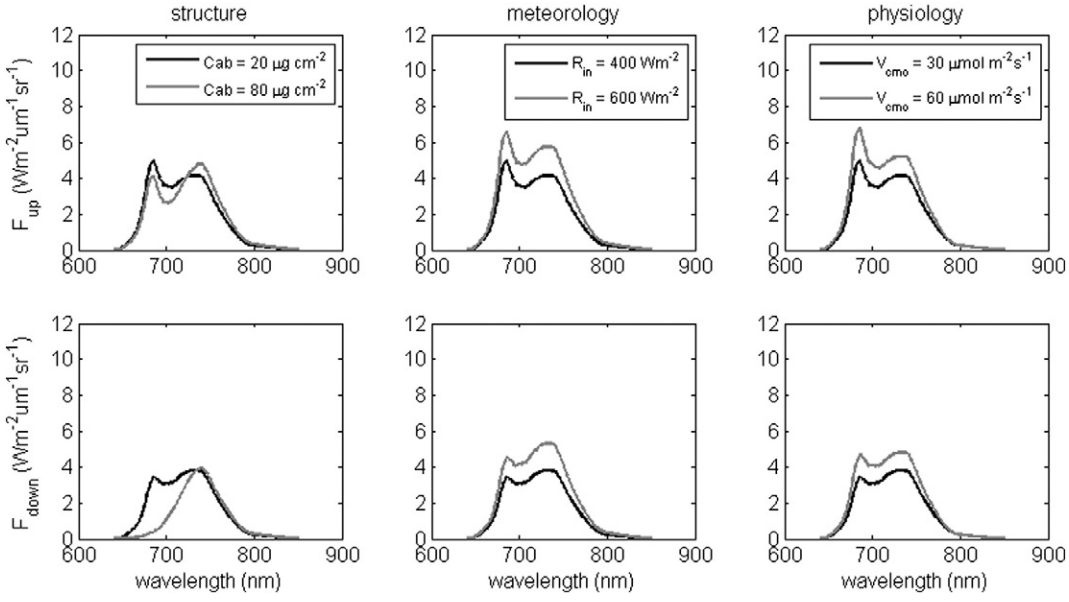

Fig. 2. Sensitivity of upward (top) and downward (bottom) leaf SIF to chlorophyll content (left), irradiance (middle) and optimum carboxylation capacity (right).

Table 1
Variables and parameters of the SCOPE model. Inputs apply to all three leaf physiological submodels (TB12-D, TB12 and MD12), unless indicated otherwise.

Input	Interpretation	Unit	Min	Max	Default
Soil					
rss	Soil resistance for evaporation	[200–5000 s m^{-1}]	200	5000	500
SMC	Volumetric soil moisture content	[0.01–0.7]	0.01	0.7	0.25
Leaf optical					
N	Mesophyll structural parameter in prospect	[−]	1	2.5	1.4
Cw	Water content in PROSPECT	g cm^{-2}	0	0.1	0.009
Cdm	Dry matter content in PROSPECT	g cm^{-2}	0	0.05	0.012
Cs	Senescence factor in PROSPECT	[−]	0	0.9	0
Cab	Chlorophyll content in PROSPECT	μg cm^{-2}	0	80	40
Leaf physiology (TB12-D, TB12, MD12)					
m	Ball–Berry stomatal conductance parameter	[−]	2	20	8
kV	Extinction coefficient for a vertical profile of V_{cmo} (maximum value of V_{cmo} occurs at the top of the canopy).	[−]	0	0.8	0.64
Rdparam	Parameter for dark respiration (Rd = Rdparam ∗ V_{cmo})	[−]	0.001	0.03	0.015
V_{cmo}	maximum carboxylation capacity (at optimum temperature)	μmol m^{-1} s^{-1}	0	200	30
Leaf physiology (MD12 only)					
kNPQs	Rate constant of sustained thermal dissipation (Porcar-Castell, 2011)	–	0	10	0
qLs	Fraction of functional reaction centers (Porcar-Castell, 2011)	–	0	1	1
Aerodynamic					
rbs	Soil boundary layer resistance	s m^{-1}	5	30	10
rwc	Within canopy layer resistance	s m^{-1}	0	20	0
rb	Leaf boundary resistance	s m^{-1}	5	20	10
Micrometeorologic					
p	Air pressure	hPa	300	1090	970
u	Wind speed	m s^{-1}	0	50	2
Oa	O_2 concentration in the air	ppm	0	220	209
ea	Atmospheric vapor pressure	hPa	0	150	15
Ca	CO_2 concentration in the air	ppm	50	1000	380
Ta	Air temperature	°C	−10	50	20
Rin	Incoming shortwave radiation	W m^{-2}	0	1400	600
Rli	Incoming longwave radiation	W m^{-2}	0	400	300
Canopy					
lw	Leaf width	m	0.01	0.1	0.1
LIDFa	LIDF parameter a, which controls the average leaf slope	[−]	−1	1	−0.35
LIDFb	LIDF parameter b, which controls the distribution's bimodality	[−]	−1	1	−0.15
LAI	Leaf area index	m^2 m^{-2}	0	7	3
hc	Canopy height	m	0.1	2	1
Geometry					
VZA	Viewing zenith angle	Degree	0	10	0
RAA	Relative azimuth angle	Degree	0	180	0
SZA	Sun zenith angle	Degree	0	60	30

On the input side, two different GSA strategies were pursued:

(1) The first strategy was suited to acquisitions over a single site with relatively consistent ecosystem attributes, as would be done, for example, by an airborne imaging spectrometer (e.g., Damm et al., 2014; Guanter et al., 2010). For a site-specific acquisition it is assumed that micrometeorological conditions are spatially constant within an acquisition, so they may be kept to default values. Also the sun-target-viewing geometry is constant and thus kept to default values. Hence, only variables directly related to vegetation are included in the analysis, that is, leaf physiological, leaf RT, and canopy variables.
(2) A second strategy was used that included all SCOPE variables, i.e., soil, leaf, physiological, aerodynamic, micrometeorological, and canopy variables. For these variables the full ranges expected to occur on Earth are used. The analysis can contribute to an improved understanding of remotely sensed acquisitions at Earth's global scale (e.g., Frankenberg et al., 2011; Joiner et al., 2011). (Near-nadir sensors are assumed.)

These two types of GSAs can help to bridge the existing gap between small scale field studies and global studies by identifying the key variables determining SIF observations at both scales. For both situations, Saltelli's method was applied for both TB12-D and MD12 modules, for C3 plants. Additionally, for the purpose of comparing the different leaf physiological modules (TB12-D and MD12), both sustained NPQ and PSII photoinhibition (kNPQs and qLs, which are relevant for seasonal changes) in the MD12 were kept fixed at their default values (in the TB12 modules, the NPQ is modeled empirically, and hence, no variation in parameters describing sustained NPQ is possible). This analysis allowed verification of whether both models delivered the same outputs. To cover the full range of vegetation conditions, the variable ranges (i.e., minima and maxima) were derived from the literature (Mousivand et al., 2014) and by expert knowledge (see Table 1). These ranges were then sampled according to Sobol's quasi-random sequence generator. Regarding the output products, in addition to SIF, the TOC reflectance was analyzed as a quality control. The spectral sampling of the simulations was adjusted to 1 nm, so for reflectance output a total of 2101 contiguous spectral bands were sampled between 400 and 2500 nm and for SIF output 160 contiguous spectral bands between 641 and 800 nm.

For each analysis, $(N(k+2))$ model simulations were run, where N is the sample size and equals 2000, and k is the number of input variables and equals 14 variables for TB12-D and 16 for MD12 for the local situation (only vegetation variables). This produced 32,000 and 36,000

simulations, respectively. For the global situation (all SCOPE variables) 30 for TB12-D and 32 for MD12 were considered, producing 64,000 and 68,000 simulations, respectively.

Prior to applying GSA to SCOPE SIF outputs, the validity of the method had to be assessed. This was done by calculating GSA over SCOPE's surface bidirectional reflectance outputs. The impact of input variables to reflectance outputs is well understood, and a GSA has been applied previously to PROSAIL models (e.g., Bowyer & Danson, 2004). In order to gain insight into the actual influence of a given variable, both the main effect (S_i) and the interaction effects have to be considered. Therefore, only total order index results (S_{Ti}) are shown. Due to the interactions, the sum of all S_{Ti} is greater than 1, and its magnitude varies as a function of wavelength. In order to compare the relative importance of S_{Ti}, for each variable across the 400–2400 nm VNIR region, S_{Ti} was normalized as a percentage.

5. Results

5.1. GSA reflectance results

Sobol's total order sensitivity index (S_{Ti}) results on surface reflectance across the 400–2400 nm region are given in Fig. 3. Despite the large number of SCOPE input variables (32 in the case of MD12, 30 in the case of TB12-D), the *STi* results revealed that only a relatively small number of variables drive the TOC bidirectional reflectance. It must be noted that SCOPE is essentially an energy-budget model whereby radiative transfer of reflectance, modeled with PROSPECT and SAIL, is only a part of the calculations. Hence, the majority of variables related to micrometeorology and plant physiology have no impact on reflectance. Uninfluential variables include the soil variables 'soil resistance for evaporation' (rss), 'volumetric soil moisture content' (SMC), and all of the biochemical and meteorological variables. SMC does not contribute to reflectance due to the fact that we used a fixed soil reflectance as input. As expected, only leaf, canopy and geometry variables exerted an impact on reflectance. Reflectance results are unaffected by the choice of the leaf physiological module, and S_{Ti} results match earlier PROSAIL GSA results (Bowyer & Danson, 2004). The similarity provides confidence that the applied GSA method is valid.

The structural variable leaf area index (LAI) was the main driver of the variation in reflectance. LAI governed over 55% of variation in reflectance at wavelengths longer than 1400 nm, and over 70% beyond 1880 nm. Its dominance may be explained by the fact that LAI is the main indicator of the presence and density of vegetation and determines radiation interception by the canopy. Even a small variation in LAI causes some change in the observed radiance, especially for low LAI values (Mousivand et al., 2014). Apart from LAI, spectral features in the visible part were controlled primarily by leaf pigment chlorophyll content (Cab) and senescent material fraction (Cs). The 400–700 nm spectral window is the photosynthetically active radiation for plants with Cab as the main absorbing pigment. Beyond ~700 nm the effect of Cab and the senescence factor gradually disappears due to the fact that Cab and other leaf pigments are transparent to infrared radiation. Leaf mesophyll structure (N) parameter and dry matter content (Cdm), on the other hand, influence the NIR spectra (700–1300 nm), with Cdm driving over 40% of the variability between 770 and 950 nm. Water content (equivalent water thickness (Cw)) had negligible impact on the visible and near-infrared spectral features, but it influenced the shortwave infrared considerably because of radiation absorption by leaf water. Cw accounted for over 30% of the output variance between 1150 and 1410 nm and increased to more than 50% between 1340 and 1390 nm. Another important structural variable was the leaf inclination distribution factor (LIDFa). As for LAI, it was influential throughout the whole spectral range, with a contribution of over 20% between 720 and 1150 nm. The remaining structural variables leaf width (lw), LIDFb, and vegetation height (hc) had only a marginal impact on reflectance (together about 2%). The other key variable in driving reflectance was solar zenith angle (SZA). Its influence was relatively stable (between 1 and 7%) across the 400–2400 nm spectral window. View zenith angle (VZA) and relative azimuth angle (RAA) had negligible impact (<0.3%), although it should be noted that only near-nadir instruments were targeted, with a VZA of up to 10° only.

5.2. GSA fluorescence results: vegetation variables only

5.2.1. Fluorescence

Whereas the above GSA served to decompose reflectance based on all SCOPE variables, in this section only vegetation variables were included. Such an exercise is relevant to small-scale local studies, e.g., using acquisitions from airborne imaging spectrometers. Given its importance for monitoring photosynthetic activity, of interest is how much of the SIF variability is explained by maximum carboxylation capacity (V_{cmo}) and how much by other leaf and canopy variables. Inspecting the S_{Ti} results of SCOPE with the semi-empirical TB12-D module (Fig. 4a) it was observed that four key variables drive SIF: chlorophyll content (Cab), V_{cmo}, and the structural variables LIDFa and LAI. These four variables explained on average 89.3% of the SIF variability across the 641–800 nm spectral window. The remaining 10.0% was explained by the fraction of senescent material (Cs), dry matter content

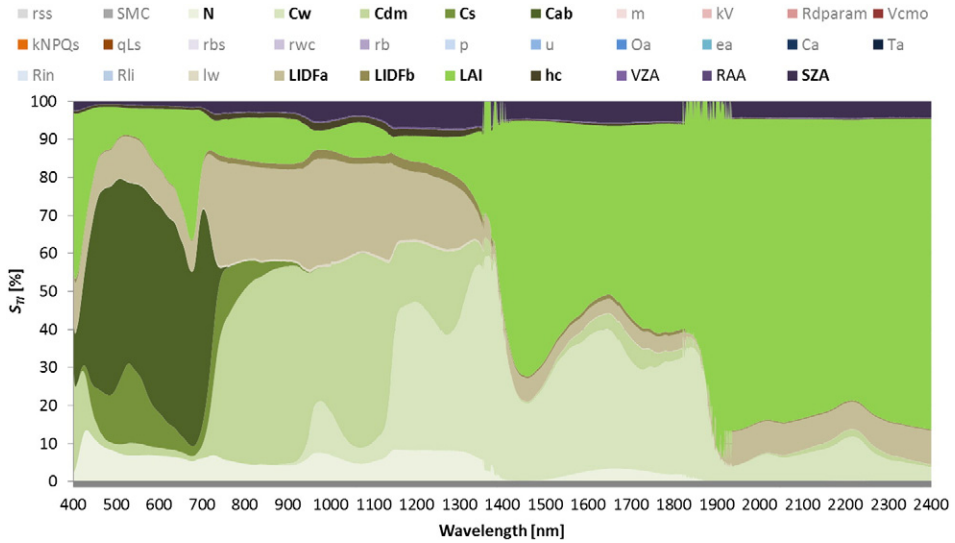

Fig. 3. GSA total sensitivity index (S_{Ti}) for SCOPE reflectance. The variables with a S_{Ti} > 1% are boldfaced; variables without any impact on reflectance are written in gray.

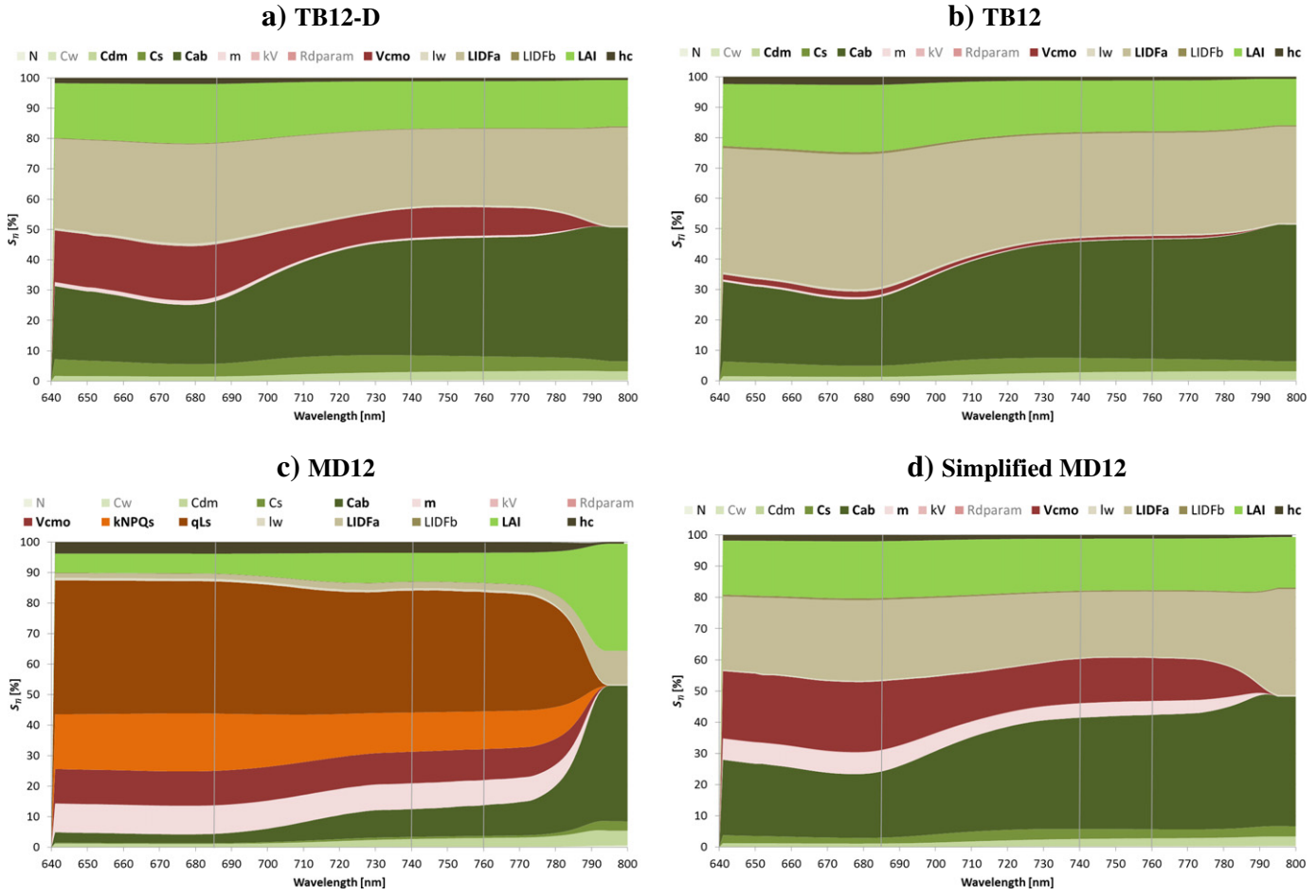

Fig. 4. GSA total sensitivity index (S_{Ti}) for SCOPE broadband SIF (641–800 nm) given only varying vegetation variables and the submodels TB12-D (a), TB12 (b) MD12 (c) and simplified MD12 without MD12-specific variables (kNPQs, qLs) (d). The variables with a $S_{Ti} > 1\%$ are boldfaced; variables without any impact on reflectance are written in gray. The vertical bars indicate the most important SIF wavelengths: the SIF_{red} and SIF_{NIR} emission peaks (685 and 740 nm), and the O_2-A absorption region (760 nm).

(Cdm), vegetation height (hc), the Ball–Berry stomatal conductance parameter (m), and leaf width (lw). The remaining variables – leaf thickness (N), leaf water content (Cw), extinction coefficient for V_{cmo} (kV), respiration (Rdparam), and LIDFb – exerted negligible influence on SIF, explaining on average only 0.6%. In the TB12-D module only 11.4% of SIF was explained by V_{cmo}, a key determinant of photosynthetic capacity. However, the relative contribution of V_{cmo} was not constant, with greater relevance in the first emission peak than the second emission peak. Its maximal contribution, 17.9%, was found at 676 nm. This suggests that in heterogeneous canopies, over 80% of the observed SIF variability may be due to variations in leaf and canopy biochemical and structural properties and their interactions rather than to variations in photosynthetic capacity. Moreover, the contribution of V_{cmo} to SIF degraded steadily at longer wavelengths. At the peak of SIF_{red} (685 nm), V_{cmo} explained 16.4%. Its contribution was considerably weaker in the second emission peak, accounting for only 9.6% of SIF variability at 740 nm, and it was further reduced to 9.3% at 760 nm (the O_2-A absorption region). At 795 nm, V_{cmo} no longer exerted any influence on the SIF signal.

When the TB12 (calibrated for non-stressed plants) leaf physiological module (Fig. 4b) was used instead of TB12-D (calibrated for plants under variable levels of drought stress), SIF was even less influenced by variations in V_{cmo}. On average, V_{cmo} contributed 1.10%, with a maximum of 1.83% at 676 nm. Variations in the fluorescence amplification factor, ε, are small in the absence of stress induced sustained NPQ (Van der Tol et al., 2014). Hence, variations in light absorption by green pigments (i.e., variations in leaf composition and canopy structure) influence SIF more than variations in the fluorescence yield (as modulated by physiological regulation) when this submodel is utilized. In fact, the SIF variability for unstressed C3 canopies was, on average 88.9%, and governed by only three key structural variables, those being Cab (33.0%), LIDFa (37.4%) and LAI (18.5%).

Using the MD12 module in SCOPE (Fig. 4c) instead introduces two additional MD12-specific variables, namely the fraction of active PSII reaction centers (qLs) and the rate constant for sustained non-photochemical quenching (kNPQs), resulting from the photoprotective retention of zeaxanthin even after dark-adaptation (Öquist & Huner, 2003). Both features have been observed to change over the season in response to cold (Gilmore & Ball, 2000; Porcar-Castell, 2011) and drought conditions (Baraldi et al., 2008), with important implications for SIF emission.

As expected, these two variables strongly determined the SIF flux: the rate constant of sustained thermal dissipation (kNPQs) and the fraction of functional reaction centers (qLs) together accounted for 51.4% of the SIF variability. Because of the dominance of the MD12-specific variables, V_{cmo} governed an average of 9.7% of the SIF variability. Apart from these leaf physiological variables, the same key leaf and canopy structural variables, i.e., Cab, LIDFa, LAI, and canopy height (hc) were influential upon the SIF flux, but to a lesser extent than with TB12-D (together 26.9%) due to the relative dominance of kNPQs and qLs.

The parameterization of ranging photodamage and photoprotection in MD12 clearly causes greater variability of the fluorescence yields. In order to compare the SCOPE sensitivity between MD12 and the TB12 modules, the sensitivity analyses has been repeated with the two

MD12-specific variables fixed (Fig. 4d). This enables a comparison of the model sensitivity with the same variables used in alternative physiological modules. With the simplified MD12 module, the same driving variables were found as before with TB12-D. But the influence of the biochemistry variables was stronger than for TB12-D, with V_{cmo} accounting for an average of 15.6% and the Ball–Berry stomatal conductance parameter (m) an average of 4.8% across the 641–800 nm spectral window, as a result of the different formulation of photosynthesis in MD12 (based on the Farquhar and von Caemmerer model, rather than the Collatz model as in TB12 and TB12-D). V_{cmo} had maximal influence at 676 nm (22.5%), and its relevance steadily decreased thereafter.

5.2.2. Fluorescence yield

The canopy level fluorescence yield, F_{yield} (hemispherical fluorescence normalized by absorbed PAR of the plants), was subject to essentially the same driving variables as the broadband fluorescence profiles. For the TB12-D module, the driving variables were Cab (25.4%), V_{cmo} (25.0%), Cs (21.5%), Cdm (11.5%) and LAI (8.3%) (Fig. 5). The structural variable LIDFa now exerted only 3.65% influence over variability, which was of similar influence as vegetation height (hc) (3.2%). The lower sensitivity to LIDFa can be explained by the fact that for F_{yield} we used the hemispherically integrated flux, which is much less influenced by the leaf inclination distribution than the fluorescence in a single (observation) direction.

Generalizing the results to physiological, leaf optical and canopy variables, the leaf optical variables determined 58.5% and the structural variables 15.3% of F_{yield} variability. F_{yield} was 25% driven by the photosynthetic variable V_{cmo}. The variables N, kV, Rdparam, and lw were non-influential. When replacing TB12-D by TB12, then the influence of leaf physiological variables was suppressed by the same driving leaf optical (65.4%) and canopy structural variables (32.0%).

Comparing those results against MD12, while keeping the MD12-specific variables fixed, the same drivers were identified, albeit with greater importance attributed to V_{cmo} (30.1%) and m (8.9%), as well as the structural variables LAI (11.7%) and hc (6.6%). These increases in relative importance were at the expense of the leaf variables Cs (which was halved), and Cdm and Cab (which were each lower by 25% compared to TB12-D).

Evaluation of MD12 with its full complement of variables revealed once again the dominance of kNPQs and qLs as drivers of F_{yield}. Together they determined 61.0% of F_{yield} variability. Other influential variables were m (11.0%), V_{cmo} (10.9%), Cab (3.9%), LAI (3.7%) and hc (2.7%).

5.3. GSA fluorescence results: all SCOPE variables

The analysis was repeated for TB12-D and MD12 including all SCOPE variables — including micrometeorological, aerodynamic and geometry inputs (Fig. 6). Such quantification is relevant to global SIF acquisitions where all these variables might be expected to influence the SIF signal and thus affect spatial SIF patterns.

Essentially the same patterns as with vegetation-only variables were revealed, but their influences were now more suppressed due to the additional influence of key micrometeorological variables. Broadband incoming shortwave radiation (Rin) was one of the most dominant variables, since F_0 is proportional to the absorbed PAR. Of secondary influence were air temperature (Ta), atmospheric vapor pressure (ea), and atmospheric CO_2 (Ca) concentration, which all affected SIF variability through ε. Also solar zenith angle (SZA) played a role.

Rin had a dominant influence throughout the whole 641–800 nm spectral window, because both F_0 of PSI and PSII are proportional to absorbed radiation. Irradiance had an additional effect on ε of (only) PSII. The influence of irradiance was therefore dominant in the first emission peak, where the PSII SIF has the largest contribution. All other micrometeorological variables only affected ε of PSII, and hence, their contribution to SIF was limited to wavelengths lower than 785 nm. When the MD12 module was used, these micrometeorological variables (particularly ea, Ta, Ca) had considerably stronger influence than when TB12-D was used. Again, this is due to the larger variability of ε in the MD12 module, largely as a result of the inclusion of the effects of photodamage and photoprotection. For TB12-D the overall effect of these micrometeorological fluctuations accounted for only 9.3% of SIF variability, compared to 23.8% for MD12. Other driving variables of SIF included Cab, LIDFa, LAI, LIDFb and hc. For TB12-D their summed average contribution to SIF variability was 49.8%, compared to 14.8% for MD12. The MD12-specific variables kNPQs and qLs contributed 27.3% to the SIF variability. The photosynthetic variable V_{cmo} contributed an average of only 2.2% (TB12-D) or 0.8% (MD12), respectively, to the full SIF signal. It is important to note that leaf physiological variables again exerted more influence in the first emission peak than in the second.

Non-influential variables were rss, SMC, N, Cw, kV, Rdparam, rbs, rcw, rb, u, Rli, lw, VZA, and RAA. Their summed averaged contribution was less than 1.7%.

Regarding F_{yield} (results not shown), besides the earlier identified driving vegetation variables (see Fig. 5), the same micrometeorological variables (Rin, Ta, ea, Ca) played a role in determining its variability.

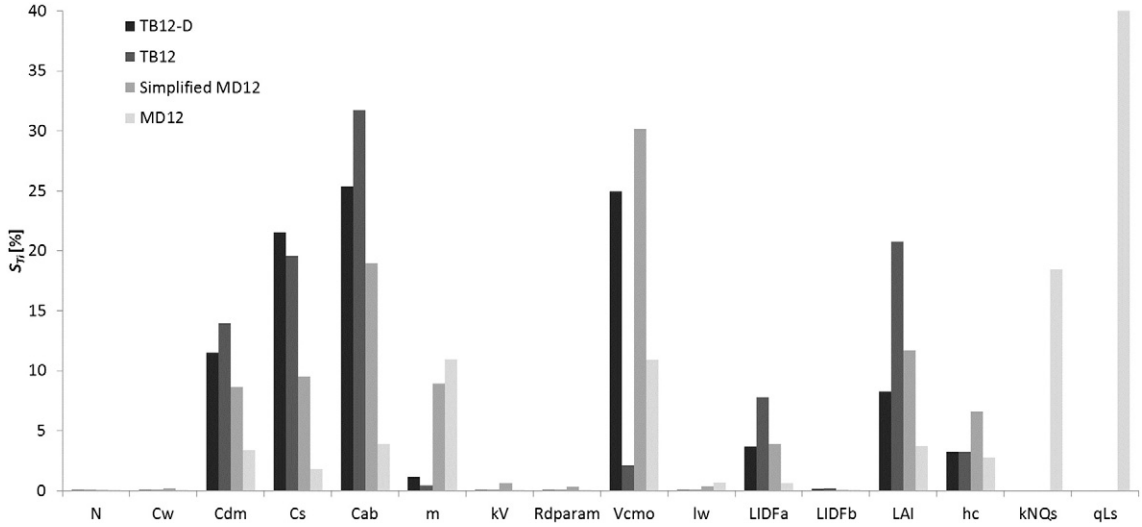

Fig. 5. GSA total sensitivity index (S_{Ti}) for SCOPE Fluorescence yield flux given only varying vegetation variables and the submodels TB12-D, TB12, simplified MD12 without MD12-specific variables (kNPQs, qLs) and MD12. Note that TB12-D, TB12 and Simplified MD12 S_{ti} results are distributed over 14 variables (Sum S_{ti} = 100%) while for MD12 over 16 variables.

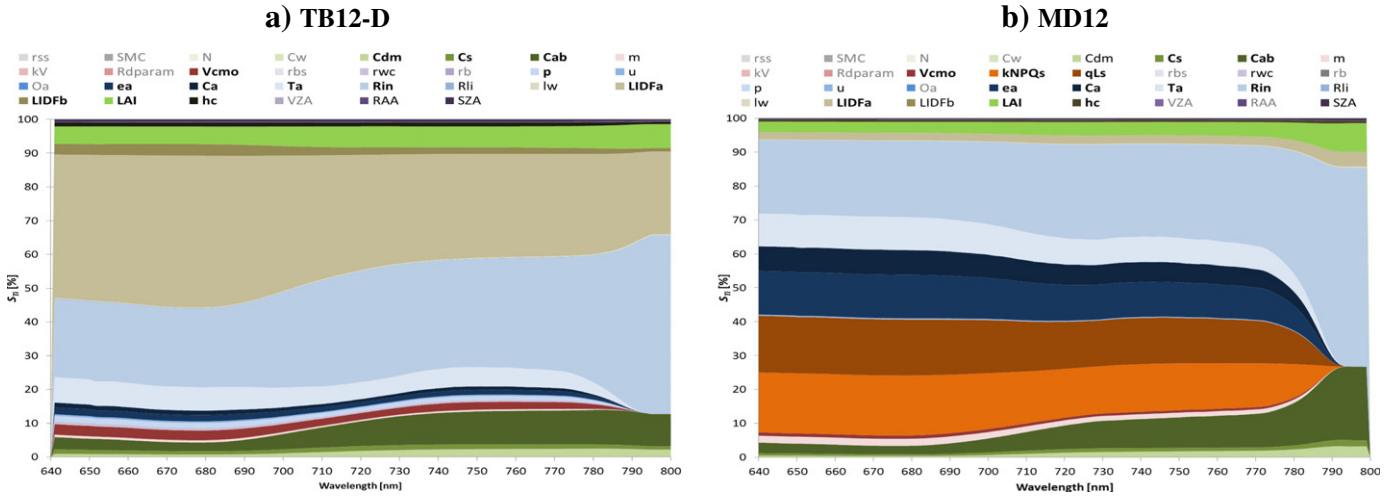

Fig. 6. GSA total sensitivity index (S_{Ti}) for SCOPE broadband SIF (641–800 nm) given all SCOPE variables and the submodels TB12-D (a), and MD12 (b). The variables with a $S_{Ti} > 1\%$ are boldfaced; variables without any impact on reflectance are written in gray. The variables with a $S_{Ti} > 1\%$ are boldfaced; variables without any impact on reflectance are written in gray.

Also here F_{yield} was more strongly related to V_{cmo} than were single SIF wavelengths: 7.57% for TB12-D and 1.92% for MD12.

6. Discussion

The main goal of this research was to disentangle and quantify the relative importance of the key variables that drive the broadband SIF signal emanating from vegetation canopies, as modeled through the fluorescence SVAT model SCOPE. A variance-based global sensitivity analysis (GSA) was applied to SCOPE SIF outputs. The output variance was decomposed into the sum of contributions of each individual input variable and the interactions (coupling terms) between different variables. Several GSA experiments were conducted in order to bridge the scaling gap between single scene and global SIF observations, i.e., varying first vegetation variables only and then varying all SCOPE variables (including micrometeorological, aerodynamic and geometry variables). Results are discussed with interpretations in a local and global context.

6.1. Varying only SCOPE vegetation variables: interpretation in a local context

By inspecting the SCOPE vegetation-only variables that drive leaf SIF emission flux propagated through the canopy, it was clear that leaf photochemistry variables only partially governed top-of-canopy SIF emission. Regardless of the chosen leaf physiological module, S_{Ti} results revealed that canopy SIF was driven largely by leaf chlorophyll content (Cab) and vegetation structure, the latter described by LAI, LIDFa and to a lesser extent vegetation height (hc). These four variables alone accounted for over 67% of the variability in SIF when considering only vegetation variables. This part of the variability is related to the absorption of PAR by chlorophyll in the vegetation, and re-absorption of the emitted SIF_{red}. V_{cmo}, the variable that indicates leaf photosynthetic capacity, drove at most up to 22.5% of the SIF emission when measured at 676 nm where its contribution is maximal (Fig. 4d). This part of the variability is related to the distribution of the absorbed PAR over heat dissipation, photochemistry and fluorescence. Hence, most of the variability of SIF is caused by variations in absorbed PAR, whereas a part of the variation is driven by variations in fluorescence emission efficiency, as quantified by the variable ε.

The emission efficiency of fluorescence ε is proportional to the excitation lifetime, which is in turn inversely proportional to the efficiency of all de-excitation processes together. The two main ones, competing with SIF, are photochemistry (resulting in electron transport and ultimately in photosynthesis) and energy-dependent heat dissipation (Baker, 2008). The two processes result in the so-called photochemical and non-photochemical quenching (i.e., reduction) of SIF. The sensitivity of SIF to biochemical regulation therefore largely depends on the capacity of plants to adjust these two de-excitation pathways in response to environmental conditions (Van der Tol et al., 2014). Despite the complex interactions between the two processes, novel models have been proposed over the last few years to capture the relationship between SIF and photochemistry alone, as captured in the more data-driven TB12 modules and in the more process-based MD12 module, as applied here. Despite the different approaches, both models capture the same general features of the relationship, in good agreement with experimental evidence (Flexas et al., 2002; Rosema, Snel, Zahn, Buurmeijer, & Van Hove, 1998): (i) a negative association between photochemical and fluorescence yields under limiting (low) light conditions, with fluorescence yield increasing with light; and (ii) a positive association between the two yields under high-light conditions (i.e., when photosynthesis is predominantly limited by CO_2 availability), as a result of the feedback on lumen pH and build-up of non-photochemical quenching (Avenson, Cruz, & Kramer, 2004). In contrast with the data-driven TB12 modules, however, the MD12 module predicts the relationship between the two yields under light-saturated conditions to be modulated by photosynthetic dark reactions (and therefore by stomatal closure or ancillary environmental conditions).

Moreover, another advantage gained with the MD12 module is that long-term changes in the photosynthetic apparatus in response to stressful conditions are taken into account, in particular PSII photodamage and zeaxanthin retention and photoprotection. The relevance of these processes is increasingly recognized for vegetation growing under natural conditions (Baker & Oxborough, 2004; Demmig-Adams & Adams, 2006). Although we are not yet in a position to model long-term responses to environmental conditions, it is important to assess their relevance in modulating leaf and canopy SIF radiance, which could provide a tool for their remote-sensing assessment.

The TB12(-D) modules describe the adjustment of de-excitation processes using a fit to experimental data; thus a number of empirical coefficients take fixed values. In contrast, the MD12 module allows more degrees of freedom, and this explains the difference in sensitivity between the models. However, the parameter values are hard to know *a priori* because the way in which the biochemical regulation varies is still largely unknown. We expect that when the problem is well constrained (irradiance and optical properties of the vegetation, which

have a large effect on SIF, are known), then the remaining variability of observed SIF could be used to evaluate the biochemical adjustment spatially by inferring the excitation lifetimes after tuning the model to measurements. However, we have not tested this and such analysis is beyond the scope of the current paper.

Chlorophyll content (Cab) and canopy structure have two different effects on SIF. On the one hand, they determine the absorption of PAR by photosystems, the main driver of photosynthesis. Leaves with a higher Cab concentration absorb more light and hence produce a higher SIF intensity within the leaf (Vogelmann & Han, 2000). On the other hand, emitted SIF is also scattered and SIF_{red} reabsorbed within the canopy. Since within-leaf light scattering occurs in all directions, SIF will be emitted from both leaf sides (Louis, Cerovic, & Moya, 2006) and propagated throughout the canopy (Van Wittenberghe, Alonso, Verrelst, Moreno, & Samson, 2015; Van Wittenberghe et al., 2013). Both effects are simulated by SCOPE. Internal reabsorption of fluoresced light in leaves and canopy occurs intensively in the red, due to the Cab absorption peak near 680 nm (Buschmann, 2007; D'Ambrosio, Szabo, & Lichtenthaler, 1992). Specifically, SIF_{red} emitted from the lower canopy region will have a high chance of interception by Cab pigments located in the surrounding canopy. Also, as light intensity decreases with canopy depth, the SIF signal intensity will decrease accordingly. This implies that the canopy-leaving SIF_{red} signal mainly originates from SIF fluxes emanating from the upper layers of relatively dense canopies. The second emission peak in NIR (with maximum around 740 nm), on the other hand, is located in the transition zone between highly absorbed red fluxes and highly scattered NIR fluxes (750–1400 nm) (Pfündel, 1998). Multiple scattering and absorption effects between different layers of foliage occur within a canopy, and these effects are influenced by plant density and architecture, typically characterized by LAI, leaf orientation (LIDFa), and vegetation height. Thus, the SIF_{NIR} (second emission peak) will be highly scattered according to vegetation structural properties (Knyazikhin et al., 2013).

Altogether, canopy structure (i.e., plant architecture and density) will determine the amount of light penetrating through the upper layers and also reabsorption and scattering effects. Within the canopy, SIF_{red} of lower canopy layers is partly reabsorbed, whereas SIF_{NIR} is scattered and contributes to the diffuse upward flux. Vegetation structure, therefore, imposes a significant impact on canopy-leaving SIF signals (Fournier et al., 2012; Miller et al., 2005). Its relative importance has been quantified here using SCOPE. Our global sensitivity analysis (GSA) confirmed that chlorophyll content, leaf and canopy structure play important roles in the SIF signal exiting the canopy. Hence, spatially explicit knowledge of key biochemical and biophysical variables is necessary in order to achieve objective interpretations of remotely sensed SIF observations.

We further found that the relative importance of the main variable driving photosynthetic activity, V_{cmo}, was not constant within the SIF 641–800 nm spectral window, likely due to the increasing contribution of PSI at longer wavelengths (see also Porcar-Castell et al., 2014). V_{cmo} was most influential in driving the SIF signal near the first emission peak, reaching a maximum at 676 nm, then decreasing towards the NIR until it disappeared at 795 nm. This gradual decline with wavelength is caused by the increasing relative contribution of PSI SIF, which has a constant ε and is independent of V_{cmo}. It should hereby be emphasized that the leaf physiological modules only affect the fluorescence yield of PSII (ε), while the radiative transfer and F_0 level of SIF in SCOPE is independent of the leaf physiological module applied. The choice of the physiological module may therefore still affect the relative sensitivity of canopy structural variables, compared to biochemical variables, even though the absolute effect of the structural parameters on SIF is unaffected. With respect to field studies that have used the O_2-A Fraunhofer line at 760 nm, results obtained here with S_{ti} for the two TB12 and MD12 leaf physiological submodels suggest that the relative importance V_{cmo} at 760 nm is only about 60% of its maximal contribution at 676 nm. This confirms experimental results by Cheng et al. (2013), who found that SIF_{red} retrievals at 688 nm had a stronger link with observed GPP than SIF_{NIR} (i.e., 757.86 nm, 760.86 nm and 772.67 nm). Our GSA also demonstrated that the influence of V_{cmo} is more dominant for F_{yield} than for SIF radiance at a single wavelength. This is encouraging for future imaging spectrometers that strive to reconstruct the full SIF signal to enable calculating F_{yield}.

The awareness that effects of leaf and canopy structure can seriously compromise the ability to estimate photosynthetic activity implies that utmost care is required in interpreting the SIF signal. Various small-scale field studies have demonstrated that variable results across vegetation types and conditions can be obtained in using SIF to estimate net photosynthesis or GPP (Damm et al., 2010; Zarco-Tejada, Morales, et al., 2013; Cheng et al., 2013). Apart from Cheng et al. (2013), these studies relied on SIF_{NIR} to establish relationships with GPP. Our GSA suggests that most of the variability found in SIF_{NIR} (and possibly also in GPP) is related to variations in Cab and vegetation structure as expressed by LAI and leaf inclination distribution. Experimental airborne studies have attempted to ascertain the potential propagated impact of these variables on SIF_{NIR} (e.g., Damm et al., 2010, 2014), or the temporal SIF dynamics of a structurally homogenous evergreen canopy (Zarco-Tejada, Morales, et al., 2013). Both studies revealed that varying vegetation properties, atmospheric conditions or sun angles in diurnal setup can be critical when interpreting SIF retrievals. But the impact of all these factors together had been left unstudied. By considering all interactions in this modeling study, the key variables that drive SIF emanating from vegetation canopies have been theoretically identified and quantified.

However, several limitations must be taken into account. It must be noted that the effect of surface heterogeneity in the horizontal direction could not be addressed with the (1D) model SCOPE. The layer concept of the model does not allow for assessing the effects of multiple scattering between, for example, tree crowns. Also, in the present study full minimum–maximum ranges of variables were used. It is evident that in the field scale not all of the variables vary over such large ranges; the relative contribution of each parameter may differ in each experiment. For example, variations in leaf inclination and leaf area within an agricultural field may be much smaller than between fields. In contrast, soil induced variations in photosynthetic parameters (soil moisture, fertilization) may not follow field boundaries. At the same time, changing atmospheric or illumination configuration (e.g., stronger light conditions) may affect biochemical-SIF relationships (Van der Tol et al., 2014, see also next section). A GSA proved to be useful to estimate the role of biochemical and structural variables in the SIF signal. But ideally the analysis is combined with *a priori* ranges of the local variability of inputs in order to reveal the site-specific driving variables.

6.2. Varying all SCOPE variables: interpretation in a global context

When taking all scope variables into account, apart from the aforementioned vegetation variables, micrometeorological variables, especially incoming shortwave radiation (Rin) – and to a lesser extent air pressure (Ta), atmospheric CO_2 concentration (Ca), and atmospheric vapor pressure (ea) – influenced the SIF flux. Solar zenith angle also had a role, albeit to an even lesser extent (≤1%). Altogether, decomposition of the SIF signal into its driving variables suggests that in heterogeneous conditions, which is the default case for observations of large land areas of the globe, over 97% of the canopy SIF variability is not caused by variations in the leaf photosynthetic capacity (V_{cmo}), but rather by other leaf, canopy and micrometeorological effects and their interactions. This implies that along with retrieving SIF it is important to characterize driving variables (Cab, LAI, LIDFa, Rin) in order to accurately relate SIF and canopy photosynthesis in a given situation.

The S_{Ti} results here suggest that the set of driving variables that affect SIF may complicate the interpretation of current global fluorescence maps. While first efforts have been presented by researchers utilizing data from atmospheric monitoring satellites (Frankenberg et al., 2011;

Guanter et al., 2012; Joiner et al., 2011), they have relied on the NIR Fraunhofer lines in the ~740–770 nm window. Given that the second peak of the SIF emission is more strongly influenced by leaf and canopy structure than is the first emission peak, it bears the consequence that spatial variations in vegetation structure impose non-trivial influences on the spatial variations of SIF_{NIR} observations. Relationships between SIF_{NIR} and GPP have been found by linear regression (e.g., Frankenberg et al., 2011; Guanter et al., 2012, 2014), and Guanter et al. (2012) suggested that these relationships likely are biome-dependent due to photochemical and canopy structural properties. Our results have actually quantified these variables and suggest that the main drivers of these relationships include Rin, Ta, Cab, LAI, and LIDFa. Several of these key variables (e.g., Rin, LAI) can be readily obtained globally with relatively high accuracy (e.g., Baret et al., 2013; Zhang, Guanter, et al., 2014). For other surface variables (e.g., Cab, LIDFa) operational retrieval schemes are only in their infancy (e.g., Verrelst, Rivera, Moreno, & Camps-Valls, 2013).

Although we did not consider GPP in the present analysis, the SCOPE model shows that the drivers of GPP largely overlap with the drivers of SIF. It is possible that the correlation between GPP and SIF found globally in other studies is due to a sensitivity of both to these driving variables. In fields where these main drivers are known, the unexplained variability in SIF could be attributed to V_{cmo} (Zhang, Guanter, et al., 2014).

Given the impact of micrometeorological effects, as well as physiological and structural influences on the TOC SIF signal, it will require effective strategies to disentangle the information content related to photosynthetic activity from that of vegetation structure in order to arrive at unbiased GPP estimations. Two strategies to address these issues may be envisaged: (1) exploitation of the full SIF emission, i.e., including both SIF_{red} and SIF_{NIR} emission features; and (2) use of jointly derived biophysical variables in order to account for structural effects. SIF_{red} and SIF_{NIR} have different features: SIF_{red} being less scattered and more sensitive to PSII photochemistry, and SIF_{NIR} being less re-absorbed. Detection of these two signals in combination with reflectance based estimates of pigments, could reveal phenological changes in canopies: the relations among Cab, V_{cmo} and LAI within fields and during the season leading to improved understanding of plant physiological responses to environmental drivers. Additional biophysical variables may be assimilated into SIF–photosynthesis relationships (Verrelst, Alonso, et al., 2013). Another point is that the larger the pixel size the higher the probability of encountering considerable variability due to leaf, canopy or micrometeorological effects within a given pixel. This is a strong argument for striving for a high spatial resolution in order to reduce within-pixel uncertainties.

In light of that argument, there are challenges for measurement of SIF from space, particularly for sensors with spatial footprints in the order of several or tens of kilometers (e.g., TANSO-FTS on board GOSAT, GOME-2 on MetOp, SCIAMACHY on EnviSat which was in operation until 2012, and TROPOMI which will be on board Sentinel-5P). In addition, sensors with restricted spectral range (e.g., OCO-2) or relatively low spectral resolution (e.g., 5–10 nm) would not be able to capture the red or NIR peaks nor the full SIF spectral emission. In comparison, the Fluorescence Explorer (FLEX) has been designed specifically to capture the SIF emission with sufficient spatial and spectral detail to allow retrieval of the red and NIR bands as well as other relevant features such as non-photochemical energy dissipation and canopy temperature. The FLEX mission is currently being evaluated as a candidate for the European Space Agency's Earth Explorer 8 mission program. FLEX, a small satellite flying in tandem with ESA's Sentinel-3, would be equipped with an imaging spectrometer (FLORIS) specifically designed to capture the full broadband SIF signal, including both emission peaks, and also the ability to derive F_{yield}. The spectral range of capture by FLORIS would be 500 to 780 nm at high spectral resolution (up to 0.3 nm) in the regions of the SIF peaks. With a continuous spatial resolution of 300 m, FLEX would provide bi-weekly global coverage of a variety of land management types and size classes (Kraft et al., 2013; Moreno, Asner, Bach, et al., 2006). The visible part of the spectrum (500–677 nm) also allows for the concurrent estimation of chlorophyll absorption and xanthophyll pigments (e.g., PRI). Relevant surface (e.g., LAI) and meteorological information will be available from Sentinel-3 to facilitate signal correction (Kraft et al., 2013), supply inputs to models such as SCOPE, and support interpretation of SIF. This novel and spatially continuous dataset at high resolution is foreseen to allow monitoring of the Earth's vegetation vitality and to link SIF with photosynthetic carbon uptake with a greater degree of confidence.

7. Conclusions

The SCOPE model (v1.53) was used here to simulate the canopy-leaving sun-induced chlorophyll fluorescence (SIF) spectrum in four steps: (1) the distribution of irradiance within the canopy, (2) the leaf SIF response to irradiance as a function of leaf composition, (3) physiological regulation of the fluorescence yield of photosystem II as a function of micrometeorological drivers and carboxylation capacity, and (4) propagation of the emitted SIF through the canopy. Modifications of the originally published version of SCOPE (Van der Tol, Verhoef, Timmermans, et al., 2009) included introduction of the leaf fluorescence model Fluspect, the addition of several leaf physiological modules for estimating fluorescence quenching in different stress conditions, and separate treatment of the two photosystems, PSI and PSII.

To quantify the relative importance of each input variable on variability of model SIF outputs, a variance-based global sensitivity analysis (GSA) based on Saltelli's method was applied. The method efficiently quantifies the relative effects of input variables on model output, as well as interactions between variables, through use of the Sobol' total order sensitivity index (S_{Ti}). The pursued strategy consists of first considering only vegetation variables, and then considering all SCOPE variables including micrometeorological and geometry variables. It led to the following conclusions:

Varying only SCOPE vegetation variables:

- Driving leaf optical and canopy structural variables were as follows: chlorophyll content (Cab), leaf inclination distribution factor (LIDFa), and leaf area index (LAI). These three variables determine the large majority of variability in SIF.
- Using an empirically calibrated model for fluorescence quenching (TB12-D) with only 4 fluorescence variables, the driving biochemical variable was the carboxylation capacity at optimum temperature, V_{cmo}. On the whole, V_{cmo} explained 11.4% of the broadband SIF variability and 25% of the F_{yield}. Consequently, the S_{ti} results suggest that in heterogeneous canopies three quarters or more of the observed fluorescence variability is not due to variations in photosynthetic capacity, but rather to variability in leaf optical and canopy structural properties.
- Using a mechanistic model for fluorescence quenching (MD12), driving variables were the rate constant of sustained thermal dissipation (kNPQs) and the fraction of functional reaction centers (qLs). When keeping the MD12-specific variables fixed the model behaved similarly as TB12-D with somewhat more emphasis on V_{cmo} (overall SIF flux of 15.6%; F_{yield}: 30.1%).
- The influence of the photosynthetic capacity variable V_{cmo} was not constant across the spectral domain. V_{cmo} had its greatest influence in the first (red) emission peak region, with a maximum at 676 nm. Two reasons for this finding could be (1) the more direct link of the red peak to PSII, and (2) because of re-absorption the signal that escaped the canopy was less prone to multiple scattering.

Varying all SCOPE variables:

- The same vegetation variables were important as on the local scale, but also the following micrometeorological variables were found to be significant drivers of the broadband SIF flux: most of all broadband

incoming shortwave radiation (Rin), followed by air temperature (Ta). These two variables alone can drive over 30% the broadband SIF flux. Other influential variables included atmospheric vapor pressure (ea) and atmospheric CO_2 concentration (Ca).

- V_{cmo} accounted for at most 2.9% in the red emission at 676 nm. This contribution was further reduced in the O_2-A absorption region or the solar Fraunhofer lines around 740–770 nm. Consequently, the S_{ti} results suggest that in heterogeneous conditions, which is inevitable at a global scale, no more than 3% of SIF variability is directly related to photosynthetic activity. However, both in conducted local and global GSA experiments, V_{cmo} played a more important role in driving F_{yield}.

In general, these findings suggest that it is more beneficial to exploit the full broadband emission flux than one band in the NIR in trying to link SIF to photosynthetic properties such as GPP. Key driving variables need to be taken into account in order to produce unbiased interpretations of SIF.

Acknowledgments

Funding for this work was provided by the European Space Agency (ESA), '2012 FLEX/Sentinel-3 Tandem Mission Photosynthesis Study' (ESA/ESTEC Contract No. 4000106396/12/NL/AF). Three anonymous reviewers are thanked for providing comments that helped to improve the quality of the original manuscript.

References

Alonso, L., Gómez-Chova, L., Vila-Francés, J., Amorós-López, J., Guanter, L., Calpe, J., et al. (2007). *Sensitivity analysis of the Fraunhofer line discrimination method for the measurement of chlorophyll fluorescence using a field spectroradiometer.*

Amoros-Lopez, J., Gomez-Chova, L., Vila-Frances, J., Alonso, L., Calpe, J., Moreno, J., et al. (2008). Evaluation of remote sensing of vegetation fluorescence by the analysis of diurnal cycles. *International Journal of Remote Sensing*, *29*, 5423–5436.

Avenson, T.J., Cruz, J.A., & Kramer, D.M. (2004). Modulation of energy-dependent quenching of excitons in antennae of higher plants. *Proceedings of the National Academy of Sciences of the United States of America*, *101*, 5530–5535.

Baker, N.R. (2008). Chlorophyll fluorescence: A probe of photosynthesis in vivo. *Annual Review of Plant Biology*, *59*, 89–113.

Baker, N.R., & Oxborough, K. (2004). Chlorophyll fluorescence as a probe of photosynthetic productivity. In G.C. Papageorgiou, & Govindjee (Eds.), *Chlorophyll a fluorescence. A signature of photosynthesis*. Dordrecht: Springer.

Ball, J. T., Woodrow, I. E., & Berry, J. A. (1991). A model predicting stomatal conductance and its contribution to the control of photosynthesis under different environmental conditions. *Progress in Photosynthesis Research* (pp. 221–224). the Netherlands: Springer.

Baraldi, R., Canaccini, F., Cortes, S., Magnani, F., Rapparini, F., Zamboni, A., et al. (2008). Role of xanthophyll cycle-mediated photoprotection in *Arbutus unedo* plants exposed to water stress during the Mediterranean summer. *Photosynthetica*, *46*, 378–386.

Baret, F., Weiss, M., Lacaze, R., Camacho, F., Makhmara, H., Pacholcyzk, P., et al. (2013). GEOV1: LAI and FAPAR essential climate variables and FCOVER global time series capitalizing over existing products. Part 1: Principles of development and production. *Remote Sensing of Environment*, *137*, 299–309.

Bonan, G.B. (1996). *A land surface model (LSM version 1.0) for ecological, hydrological, and atmospheric studies: Technical description and user's guide. NCAR Technical Note NCAR/TN-417 + STR.*

Bowyer, P., & Danson, F.M. (2004). Sensitivity of spectral reflectance to variation in live fuel moisture content at leaf and canopy level. *Remote Sensing of Environment*, *92*, 297–308.

Buschmann, C. (2007). Variability and application of the chlorophyll fluorescence emission ratio red/far-red of leaves. *Photosynthesis Research*, *92*, 261–271.

Campolongo, F., Saltelli, A., & Cariboni, J. (2011). From screening to quantitative sensitivity analysis. A unified approach. *Computer Physics Communications*, *182*, 978–998.

Cariboni, J., Gatelli, D., Liska, R., & Saltelli, A. (2007). The role of sensitivity analysis in ecological modelling. *Ecological Modelling*, *203*, 167–182.

Cheng, Y., Middleton, E., Zhang, Q., Huemmrich, K., Campbell, P., Corp, L., et al. (2013). Integrating solar induced fluorescence and the photochemical reflectance index for estimating gross primary production in a cornfield. *Remote Sensing*, *5*, 6857–6879.

Collatz, G.J., Ball, J.T., Grivet, C., & Berry, J.A. (1991). Physiological and environmental regulation of stomatal conductance, photosynthesis and transpiration: A model that includes a laminar boundary layer. *Agricultural and Forest Meteorology*, *54*, 107–136.

Collatz, G.J., Ribas-Carbo, M., & Berry, J.A. (1992). Coupled photosynthesis–stomatal conductance model for leaves of C4 plants. *Australian Journal of Plant Physiology*, *19*, 519–538.

Cowan, I.R., & Farquhar, G.D. (1977). Stomatal function in relation humidity. *Plant, Cell and Environment*, *18*, 357–364 (Symposium of the Society for Experimental Biology 31, 471–505).

Cukier, R.I., Fortuin, C.M., Shuler, K.E., Petschek, A.G., & Schaibly, J.H. (1973). Study of the sensitivity of coupled reaction systems to uncertainties in rate coefficients. I: Theory. *The Journal of Chemical Physics*, *59*, 3873–3878.

D'Ambrosio, N., Szabo, K., & Lichtenthaler, H.K. (1992). Increase of the chlorophyll fluorescence ratio F690/F735 during the autumnal chlorophyll breakdown. *Radiation and Environmental Biophysics*, *31*, 51–62.

Damm, A., Elber, J., Erler, A., Gioli, B., Hamdi, K., Hutjes, R., et al. (2010). Remote sensing of sun-induced fluorescence to improve modeling of diurnal courses of gross primary production (GPP). *Global Change Biology*, *16*, 171–186.

Damm, A., Erler, A., Hillen, W., Meroni, M., Schaepman, M.E., Verhoef, W., et al. (2011). Modeling the impact of spectral sensor configurations on the FLD retrieval accuracy of sun-induced chlorophyll fluorescence. *Remote Sensing of Environment*, *115*, 1882–1892.

Damm, A., Guanter, L., Laurent, V.C.E., Schaepman, M.E., Schickling, U., & Rascher, U. (2014). FLD-based retrieval of sun-induced chlorophyll fluorescence from medium spectral resolution airborne spectroscopy data. *Remote Sensing of Environment*, 256–266.

Daumard, F., Goulas, Y., Champagne, S., Fournier, A., Ounis, A., Olioso, A., et al. (2012). Continuous monitoring of canopy level sun-induced chlorophyll fluorescence during the growth of a sorghum field. *IEEE Transactions on Geoscience and Remote Sensing*, *50*, 4292–4300.

Dayyoub, A. (2011). *Novel techniques for the remote sensing of photosynthetic processes.* PhD Thesis Italy: University of Bologna.

Demmig-Adams, B., & Adams, W.W., III (2006). Photoprotection in an ecological context: The remarkable complexity of thermal energy dissipation. *New Phytologist*, *172*, 11–21.

Drusch, M., & FLEX-Team (2008). *FLEX report for assessment.* Noordwijk (The Netherlands): ESA-ESTEC (ESA SP-1313/4).

European Space Agency (2014). Earth observation portal, satellite missions. https://eoportal.org

Farquhar, G.D., von Caemmerer, S., & Berry, J.A. (1980). A biochemical model of photosynthetic CO_2 assimilation in leaves of C_3 species. *Planta*, *149*, 78–90.

Flexas, J., Escalona, J.M., Evain, S., Gulias, J., Moya, I., Osmond, C.B., et al. (2002). Steady-state chlorophyll fluorescence (Fs) measurements as a tool to follow variations of net CO(2) assimilation and stomatal conductance during water-stress in C(3) plants. *Physiologia Plantarum*, *114*, 231–240.

Fournier, A., Daumard, F., Champagne, S., Ounis, A., Goulas, Y., & Moya, I. (2012). Effect of canopy structure on sun-induced chlorophyll fluorescence. *ISPRS Journal of Photogrammetry and Remote Sensing*, *68*, 112–120.

Franck, F., Juneau, P., & Popovic, R. (2002). Resolution of the photosystem I and photosystem II contributions to chlorophyll fluorescence of intact leaves at room temperature. *Biochimica et Biophysica Acta — Bioenergetics*, *1556*, 239–246.

Frankenberg, C., Fisher, J.B., Worden, J., Badgley, G., Saatchi, S.S., Lee, J.E., et al. (2011). New global observations of the terrestrial carbon cycle from GOSAT: Patterns of plant fluorescence with gross primary productivity. *Geophysical Research Letters*, *38*.

Gamon, J.A., Penuelas, J., & Field, C.B. (1992). A narrow-waveband spectral index that tracks diurnal changes in photosynthetic efficiency. *Remote Sensing of Environment*, *41*, 35–44.

Gilmore, A.M., & Ball, M.C. (2000). Protection and storage of chlorophyll in overwintering evergreens. *Proceedings of the National Academy of Sciences of the United States of America*, *97*, 11098–11101.

Guanter, L., Alonso, L., Gomez-Chova, L., Meroni, M., Preusker, R., Fischer, J., et al. (2010). Developments for vegetation fluorescence retrieval from spaceborne high-resolution spectrometry in the O(2)-A and O(2)-B absorption bands. *Journal of Geophysical Research-Atmospheres*, *115*.

Guanter, L., Frankenberg, C., Dudhia, A., Lewis, P.E., Gómez-Dans, J., Kuze, A., et al. (2012). Retrieval and global assessment of terrestrial chlorophyll fluorescence from GOSAT space measurements. *Remote Sensing of Environment*, *121*, 236–251.

Guanter, L., Zhang, Y.G., Jung, M., Joiner, J., Voigt, M., Berry, J.A., et al. (2014). Global and time-resolved monitoring of crop photosynthesis with chlorophyll fluorescence. *Proceedings of the National Academy of Sciences of the United States of America*, *111*, E1327–E1333.

Jacquemoud, S., & Baret, F. (1990). PROSPECT: A model of leaf optical properties spectra. *Remote Sensing of Environment*, *34*, 75–91.

Jansen, M.J.W. (1999). Analysis of variance designs for model output. *Computer Physics Communications*, *117*, 35–43.

Joiner, J., Yoshida, Y., Vasilkov, A.P., Yoshida, Y., Corp, L.A., & Middleton, E.M. (2011). First observations of global and seasonal terrestrial chlorophyll fluorescence from space. *Biogeosciences*, *8*, 637–651.

Knyazikhin, Y., Schull, M., Stenberg, P., Mattus, M., Rautiainen, M., Yang, Y., et al. (2013). Hyperspectral remote sensing of foliar nitrogen content. *Proceedings of the National Academy of Sciences of the United States of America*, *110*(3) (1168, 811–812 + E185–E192).

Kraft, S., Del Bello, U., Drusch, M., Gabriele, A., Harnisch, B., & Moreno, J. (2013). On the demands on imaging spectrometry for the monitoring of global vegetation fluorescence from space. *SPIE Proceedings*, *8870*, 88700N–88712N.

Krause, G.H., & Weis, E. (1991). Chlorophyll fluorescence and photosynthesis — The basics. *Annual Review of Plant Physiology and Plant Molecular Biology*, *42*, 313–349.

Kucherenko, S., Rodriguez-Fernandez, M., Pantelides, C., & Shah, N. (2009). Monte Carlo evaluation of derivative based global sensitivity measures. *Reliability Engineering & System Safety*, *94*, 1135–1148.

Leuning, R. (1997). Scaling to a common temperature improves the correlation between the photosynthesis parameters J_{max} and V_{cmax}. *Journal of Experimental Botany*, *48*, 345–347.

Lichtenthaler, H.K., & Rinderle, U. (1988). The role of chlorophyll fluorescence in the detection of stress conditions in plants. *CRC Critical Reviews in Analytical Chemistry*, *19*, 29–85.

Louis, J., Ounis, A., Ducruet, J. -M., Evain, S., Laurila, T., Thum, T., et al. (2005). Remote sensing of sunlight-induced chlorophyll fluorescence and reflectance of scots pine in the boreal forest during spring recovery. *Remote Sensing of Environment*, *96*, 37–48.

Louis, J., Cerovic, Z. G., & Moya, I. (2006). Quantitative study of fluorescence excitation and emission spectra of bean leaves. *Journal of Photochemistry and Photobiology B — Biology*, *85*, 65–71.

Magnani, F., Olioso, A., Demarty, J., Germain, V., Verhoef, W., Moya, I., et al. (2009). *Assessment of vegetation photosynthesis through observation of solar induced fluorescence from space.* ESTEC Contract No. 20678/07/NL/HE, Final Report.

Malenovský, Z., Mishra, K.B., Zemek, F., Rascher, U., & Nedbal, L. (2009). Scientific and technical challenges in remote sensing of plant canopy reflectance and fluorescence. *Journal of Experimental Botany*, *60*, 2987–3004.

Meroni, M., Barducci, A., Cogliati, S., Castagnoli, F., Rossini, M., Busetto, L., et al. (2011). The hyperspectral irradiometer, a new instrument for long-term and unattended field spectroscopy measurements. *Review of Scientific Instruments*, *82*, 043106.

Meroni, M., Busetto, L., Colombo, R., Guanter, L., Moreno, J., & Verhoef, W. (2010). Performance of spectral fitting methods for vegetation fluorescence quantification. *Remote Sensing of Environment*, *114*, 363–374.

Meroni, M., Rossini, M., Guanter, L., Alonso, L., Rascher, U., Colombo, R., et al. (2009). Remote sensing of solar-induced chlorophyll fluorescence: Review of methods and applications. *Remote Sensing of Environment*, *113*, 2037–2051.

Miller, J.R., Berger, M., Alonso, L., Cerovic, Z., Goulas, Y., Jacquemoud, S., et al. (2003). Progress on the development of an integrated canopy fluorescence model. *International Geoscience and Remote Sensing Symposium, IGARSS'03, vol. 1.* (pp. 601–603). Toulouse, France: Institute of Electrical and Electronics Engineers Inc. (IEEE) (21–25/7/2004. ISBN 0-7803-7929-2 - 0-7803-7930-6).

Miller, J.R., Berger, M., Goulas, Y., Jacquemoud, S., Louis, J., Mohammed, G., et al. (2005). *Development of a vegetation fluorescence canopy model — Final report.*

Mohammed, G.H., Goulas, Y., Magnani, F., Moreno, J., Olejníčková, J., Rascher, U., et al. (2014). *2012 FLEX/sentinel-3 tandem mission photosynthesis study.* Final report. ESTEC contract no. 4000106396/12/NL/AF.

Moreno, J., Asner, G.P., Bach, H., et al. (2006). Fluorescence explorer (FLEX): An optimized payload to map vegetation photosynthesis from space. *AIAA 57th International Astronautical Congress, vol. 3.* (pp. 2065–2074). Valencia: IAC.

Mousivand, A., Menenti, M., Gorte, B., & Verhoef, W. (2014). Global sensitivity analysis of the spectral radiance of a soil–vegetation system. *Remote Sensing of Environment*, *145*, 131–144.

Moya, I., Daumard, F., Moise, N., Ounis, A., & Goulas, Y. (2006). First airborne multiwavelength passive chlorophyll fluorescence measurements over La Mancha (Spain) fields. *2nd International Symposium on Recent Advances in Quantitative Remote Sensing* (pp. 820–825).

Nossent, J., Elsen, P., & Bauwens, W. (2011). Sobol' sensitivity analysis of a complex environmental model. *Environmental Modelling and Software*, *26*, 1515–1525.

Öquist, G., & Huner, N.P.A. (2003). Photosynthesis of overwintering evergreen plants. *Annual Review of Plant Biology*, *54*, 329–355.

Papageorgiou, G.C., & Govindjee (2004). *Chlorophyll a fluorescence — A signature of photosynthesis.* Springer, 818.

Pedrós, R., Goulas, Y., Jacquemoud, S., Louis, J., & Moya, I. (2010). FluorMODleaf: A new leaf fluorescence emission model based on the PROSPECT model. *Remote Sensing of Environment*, *114*, 155–167.

Pedrós, R., Jacquemoud, S., Goulas, Y., Louis, J., & Moya, I. (2004). A new leaf fluorescence model. *2nd International Workshop on Remote Sensing of Solar Induced Vegetation Fluorescence, 17–19 November. Canada: Montreal.*

Pedrós, R., Moya, I., Goulas, Y., & Jacquemoud, S. (2008). Chlorophyll fluorescence emission spectrum inside a leaf. *Photochemical and Photobiological Sciences*, *7*, 498–502.

Perez-Priego, O., Zarco-Tejada, P.J., Miller, J.R., Sepulcre-Canto, G., & Fereres, E. (2005). Detection of water stress in orchard trees with a high-resolution spectrometer through chlorophyll fluorescence in-filling of the O-2-A band. *IEEE Transactions on Geoscience and Remote Sensing*, *43*, 2860–2869.

Pfündel, E. (1998). Estimating the contribution of photosystem I to total leaf chlorophyll fluorescence. *Photosynthesis Research*, *56*, 185–195.

Porcar-Castell, A. (2011). A high-resolution portrait of the annual dynamics of photochemical and non-photochemical quenching in needles of Pinus sylvestris. *Physiologia Plantarum*, *143*(2), 139–153.

Porcar-Castell, A., Tyystjärvi, E., Atherton, J., Van der Tol, C., Flexas, J., Pfündel, E.E., et al. (2014). Linking chlorophyll a fluorescence to photosynthesis for remote sensing applications: Mechanisms and challenges. *Journal of Experimental Botany*, *65*(15), 4065–4095.

Rascher, U., Agati, G., Alonso, L., Cecchi, G., Champagne, S., Colombo, R., et al. (2009). CEFLES2: The remote sensing component to quantify photosynthetic efficiency from the leaf to the region by measuring sun-induced fluorescence in the oxygen absorption bands. *Biogeosciences*, *6*, 1181–1198.

Rautiainen, M., Heiskanen, J., Eklundh, L., Mottus, M., Lukes, P., & Stenberg, P. (2010). Ecological applications of physically based remote sensing methods. *Scandinavian Journal of Forest Research*, *25*, 325–339.

Rosema, A., Snel, J.F.H., Zahn, H., Buurmeijer, W.F., & Van Hove, L.W.A. (1998). The relation between laser-induced chlorophyll fluorescence and photosynthesis. *Remote Sensing of Environment*, *65*(2), 143–154.

Saltelli, A. (2002). Making best use of model evaluations to compute sensitivity indices. *Computer Physics Communications*, *145*, 280–297.

Saltelli, A., & Annoni, P. (2010). How to avoid a perfunctory sensitivity analysis. *Environmental Modelling and Software*, *25*, 1508–1517.

Saltelli, A., Annoni, P., Azzini, I., Campolongo, F., Ratto, M., & Tarantola, S. (2010). Variance based sensitivity analysis of model output. Design and estimator for the total sensitivity index. *Computer Physics Communications*, *181*, 259–270.

Saltelli, A., Ratto, M., Andres, T., Campolongo, F., Cariboni, J., Gatelli, D., et al. (2008). *Global sensitivity analysis: The primer.* John Wiley & Sons, Ltd.

Saltelli, A., Tarantola, S., & Chan, K.P.S. (1999). A quantitative model-independent method for global sensitivity analysis of model output. *Technometrics*, *41*, 39–56.

Sellers, P. J., Berry, J. A., Collatz, G. J., Field, C. B., & Hall, F. G. (1992). Canopy reflectance, photosynthesis, and transpiration. *III. A reanalysis using improved leaf models and a new canopy integration scheme. Remote Sensing of Environment*, *42*, 187–216.

Sellers, P.J., Randall, D.A., Collatz, G.J., Berry, J.A., Field, C.B., Dazlich, D.A., et al. (1996). A revised land surface parameterization (SiB2) for atmospheric GCMs. Part I: Model formulation. *Journal of Climate*, *9*(4), 676–705.

Sobol', I.M. (1967). On the distribution of points in a cube and the approximate evaluation of integrals. *USSR Computational Mathematics and Mathematical Physics*, *7*, 86–112.

Sobol', I.M. (1990). On sensitivity estimation for nonlinear mathematical models. *Matematicheskoe Modelirovanie*, *2*, 112–118.

Song, X., Bryan, B.A., Paul, K.I., & Zhao, G. (2012). Variance-based sensitivity analysis of a forest growth model. *Ecological Modelling*, *247*, 135–143.

Srivastava, A., Greppin, H., & Strasser, R.J. (1995). The steady state chlorophyll a fluorescence exhibits in vivo an optimum as a function of light intensity which reflects the physiological state of the plant. *Plant & Cell Physiology*, *36*, 839–848.

Stuckens, J., Verstraeten, W.W., Delalieux, S., Swennen, R., & Coppin, P. (2009). A dorsiventral leaf radiative transfer model: Development, validation and improved model inversion techniques. *Remote Sensing of Environment*, *113*, 2560–2573.

Van der Tol, C., Berry, J.A., Campbell, P.K.E., & Rascher, U. (2014). Models of fluorescence and photosynthesis for interpreting measurements of solar induced chlorophyll fluorescence. *Journal of Geophysical Research, Biogeosciences*, *119*, 2312–2327.

Van der Tol, C., Verhoef, W., & Rosema, A. (2009). A model for chlorophyll fluorescence and photosynthesis at leaf scale. *Agricultural and Forest Meteorology*, *149*, 96–105.

Van der Tol, C., Verhoef, W., Timmermans, J., Verhoef, A., & Su, Z. (2009). An integrated model of soil-canopy spectral radiances, photosynthesis, fluorescence, temperature and energy balance. *Biogeosciences*, *6*, 3109–3129.

Van Wittenberghe, S., Alonso, L., Verrelst, J., Hermans, I., Delegido, J., Veroustraete, F., et al. (2013). Upward and downward solar-induced chlorophyll fluorescence yield indices of four tree species as indicators of traffic pollution in Valencia. *Environmental Pollution*, *173*, 29–37.

Van Wittenberghe, S., Alonso, L., Verrelst, J., Moreno, J., & Samson, R. (2015). Bidirectional sun-induced chlorophyll fluorescence emission is influenced by leaf structure and light scattering properties — A bottom–up approach. *Remote Sensing of Environment*, *158*, 169–179.

Verhoef, W. (1984). Light scattering by leaf layers with application to canopy reflectance modeling: The SAIL model. *Remote Sensing of Environment*, *16*, 125–141.

Verhoef, W. (2004). Extension of SAIL to model solar-induced canopy fluorescence spectra. *2nd International Workshop on Remote Sensing of Solar Induced Vegetation Fluorescence, 17–19 Nov. Canada: Montreal.*

Verrelst, J., Muñoz, J., Alonso, L., Delegido, J., Rivera, J. P., Camps-Valls, G., et al. (2012). Machine learning regression algorithms for biophysical parameter retrieval: Opportunities for sentinel-2 and -3. *Remote Sensing of Environment*, *118*, 127–139.

Verrelst, J., Alonso, L., Rivera Caicedo, J.P., Moreno, J., & Camps-Valls, G. (2013). Gaussian process retrieval of chlorophyll content from imaging spectroscopy data. *IEEE Journal of Selected Topics in Applied Earth Observations and Remote Sensing*, *6365271*, 867–874.

Verrelst, J., Rivera, J.P., Moreno, J., & Camps-Valls, G. (2013). Gaussian processes uncertainty estimates in experimental Sentinel-2 LAI and leaf chlorophyll content retrieval. *ISPRS Journal of Photogrammetry and Remote Sensing*, *86*, 157–167.

Vogelmann, T.C., & Han, T. (2000). Measurement of gradients of absorbed light in spinach leaves from chlorophyll fluorescence profiles. *Plant, Cell and Environment*, *23*, 1303–1311.

Von Caemmerer, S. (2013). Steady-state models of photosynthesis. *Plant, Cell & Environment*, *36*(9), 1617–1630.

Wainwright, H.M., Finsterle, S., Jung, Y., Zhou, Q., & Birkholzer, J.T. (2014). Making sense of global sensitivity analyses. *Computers and Geosciences*, *65*, 84–94.

Xu, C., & Gertner, G. (2007). Extending a global sensitivity analysis technique to models with correlated parameters. *Computational Statistics and Data Analysis*, *51*, 5579–5590.

Yang, J. (2011). Convergence and uncertainty analyses in Monte-Carlo based sensitivity analysis. *Environmental Modelling and Software*, *26*, 444–457.

Zarco-Tejada, P.J., Catalina, A., González, M.R., & Martín, P. (2013). Relationships between net photosynthesis and steady-state chlorophyll fluorescence retrieved from airborne hyperspectral imagery. *Remote Sensing of Environment*, *136*, 247–258.

Zarco-Tejada, P.J., Gonzalez-Dugo, V., & Berni, J.A.J. (2012). Fluorescence, temperature and narrow-band indices acquired from a UAV platform for water stress detection using a micro-hyperspectral imager and a thermal camera. *Remote Sensing of Environment*, *117*, 322–337.

Zarco-Tejada, P.J., Morales, A., Testi, L., & Villalobos, F.J. (2013). Spatio-temporal patterns of chlorophyll fluorescence and physiological and structural indices acquired from hyperspectral imagery as compared with carbon fluxes measured with eddy covariance. *Remote Sensing of Environment*, *133*, 102–115.

Zhang, Y., Guanter, L., Berry, J.A., Joiner, J., van der Tol, C., Huete, A., et al. (2014). Estimation of vegetation photosynthetic capacity from space-based measurements of chlorophyll fluorescence for terrestrial biosphere models. *Global Change Biology*, *20*, 3727–3742.